On the Loops-to-Bridges Ratio in Ordered Triblock Copolymers: An Investigation by Dielectric Relaxation Spectroscopy and Computer Simulations

K. Karatasos[†] and S. H. Anastasiadis*[,‡]

Foundation for Research and Technology−Hellas, Institute of Electronic Structure and Laser, P.O. Box 1527, 71110 Heraklion, Crete, Greece

T. Pakula

Max-Planck-Institut für Polymerforschung, P.O. Box 3148, D-55021 Mainz, Germany

H. Watanabe

Kyoto University, Institute for Chemical Research, Uji, Kyoto 611-0011, Japan

Received August 16, 1999; Revised Manuscript Received October 22, 1999

ABSTRACT: Dielectric relaxation spectroscopy and computer simulations have been used to elaborate on the loops/bridges population ratio in ordered poly(styrene-*block*-*cis*-isoprene-*block*-styrene), PS−PI−PS, triblock copolymer lamellae. The dynamics of the PI blocks are examined dielectrically for a PS−PI−PS copolymer having symmetrically inverted dipoles along the midblock backbone together with its diblock PS−PI precursor; the present work is an extension of a previous attempt (Watanabe, H. *Macromolecules* **1995**, *28*, 5006) addressing the loop/bridge ratio on the basis of a difference in the dynamics of these chains. The experiments indicate that the relaxation of the PS−PI−PS triblock lamella at $T < T_g^{PS}$ is significantly affected by preannealing at $T > T_g^{PS}$, whereas the relaxation of the PS−PI lamella is insensitive to this annealing. These results as well as changes in the data for the triblock lamella with the sample preparation method should be related to structural changes occurring only for the triblock lamella, i.e., changes in the loop/bridge population distribution as well as formation of mutually knotted loops/bridges on annealing/sample preparation. In the computer simulations, equal mobilities are assumed for the PS and PI blocks, and thus, the PS−PI junctions are allowed to move rather freely under the segregation potential. The equilibrium bridge fraction is estimated and, in agreement with theoretical predictions, is found in the range of 0.50−0.37 as the molecular weight increases. The computer simulations suggest that the relaxation intensity of loops is almost twice that of bridges with both, however, having similar relaxation rates. The dynamics of loops and bridges are found not very different from that of the diblocks (except for the lowest molecular weight); however, the total intensity for the triblocks at equilibrium is much larger than that for the respective diblocks, which may be related to the observed increase of the intensity of the triblock lamella on annealing. However, the dielectric behavior of the diblock and triblock lamellae observed for $T < T_g^{PS}$ was not explained from the simulation. These results, indicating an important influence of the junction mobility on the block dynamics, in turn suggest that the (unknotted) loops and bridges can be dielectrically distinguished only when the junction motion is essentially frozen in order to enhance the thermodynamic effect on the block motion due to the density-preserving requirement.

I. Introduction

Block copolymers exhibit a rich variety of structured mesophases when the different blocks are incompatible. The interest of the scientific community[1] was mostly focused on diblock copolymers A_nB_m, where the chemical dissimilarity between the A and B species (expressed via the segment−segment Flory−Huggins interaction parameter, χ) lead to ordered mesophases possessing various symmetries depending on the overall volume fraction of the A block, f, and on the degree of incompatibility, χN, where N is the overall number of segments; for symmetric systems ($f \cong 0.5$ or $n \cong m$), a lamellar morphology has been established for values of χN higher than ∼O(10).

Triblock copolymers, on the other hand, have received less attention, although many commercial applications requiring mechanical strength rely principally upon ordered BAB triblocks.[2] It has been established that the well-ordered mesophases formed by $B_mA_{2n}B_m$ triblocks are, in certain aspects, indistinguishable from those formed by the respective A_nB_m diblocks (e.g., their long period and symmetry are identical[3−7]), whereas a recent study showed that the effective interfacial widths are different in the two cases.[8] On the other hand, the order−disorder transition occurs at higher values of χN for the $B_mA_{2n}B_m$ triblocks than that for the A_nB_m counterparts (N is the total number of segments); i.e., the presence of two A−B junctions per triblock chain makes the system more compatible.[9−11]

It is this different chain architecture that results in a fundamental difference between the ordered mesophases of a triblock versus those of a diblock copolymer formed by cutting the triblocks in half. Whereas both blocks of the diblock as well as the two end-blocks of a triblock copolymer are each grafted at an interface by only one end and can be considered as forming dense brushes extending into their respective microdomains, the midblocks of an ordered triblock are tethered at both ends, and therefore, there are two kinds of possible conformations that the A blocks can attain: a loop conformation in which both ends are attached to the same interface and a conformation in which the two end-

* To whom correspondence should be addressed.
[†] Present address: University of Leeds, Department of Physics and Astronomy, Leeds LS2 9JT, U.K.
[‡] Also at University of Crete, Physics Department, 710 03 Heraklion Crete, Greece.

10.1021/ma991397y CCC: $19.00
Published on Web 12/29/1999

blocks reside on opposite B microdomains, and thus, the A midblock forms a bridge connecting different B domains. This qualitative distinction is of particular interest because these bridges, which may be thought of as physical cross-links connecting adjacent B microdomains, are believed to alter the mechanical and physical properties of a triblock melt from those of a diblock,[12,10] whereas the loops-to-bridges ratio, introduced as a parameter in micromechanical models,[13] may affect the macroscopic properties (e.g., the shear modulus).

Recently, theoretical efforts have been undertaken[6,7,14−17] to evaluate the fraction of loops and bridges in ordered triblock lamellae, whereas earlier theoretical investigations had concentrated on the structure of BAB triblocks.[5,18] Zhulina and Halperin[15] used a self-consistent field theory in the limit of strong segregation and, by assuming that only a very small fraction of A midblocks adopt a bridge conformation, calculated analytically the bridging fraction, $\phi_{\text{bridges}} \propto (\chi N)^{-1/9}$; this was in agreement with a different scaling analysis,[14] with the work of Matsen[16] but only in the limit of very high $\chi N \sim O(10^6)$ and with a recent estimate.[17] However, for reasonable degrees of incompatibility, χN, the fraction of midblock bridges depends only weakly on χN and for symmetric triblocks assumes values of $\phi_{\text{bridge}} \cong 0.4$ in the work of Matsen and co-workers[6,16] and $\phi_{\text{bridge}} \cong 0.63$ in the work of Jones et al.[7] for $\chi N \sim 100$ (they suggest that a renormalized fraction $q' \cong 0.46$ should be used instead of the fraction $\phi_{\text{bridge}} = q \cong 0.63$). Moreover, Matsen and Schick[6] also noted that, within the approximation employed by the midblock performing a random walk in a field symmetric about the midplane of the A lamellae, the fraction of bridges must always be less than 0.5.

On the experimental front, although various structural[4] and rheological[10] findings were tentatively attributed to the different contributions of the bridge and loop midblock conformations, quantitative determination of the bridge fraction in ordered triblocks has eluded the scientists in the field. Recently, Watanabe[19] attempted to provide an answer to the bridge fraction question using dielectric relaxation spectroscopy on a polystyrene (PS)−*cis*-polyisoprene (PI)−polystyrene symmetric triblock that was specifically synthesized to have symmetrically inverted dipoles along the backbone of the middle polyisoprene block. *cis*-Polyisoprene is one of the few polymers that possess a component of the dipole moment along the chain backbone (classified as type-A chains[20]). For usual PI chains having these dipole components aligned in the same direction along the chain backbone, the polarization is proportional to the PI end-to-end vector **R**, and the global chain motion inducing fluctuations in **R** is dielectrically detected (the component of the dipole moment perpendicular to the PI backbone leads to the dielectric observation of the local segmental motion at frequencies much faster than those of the global chain motion). This feature of PI has been extensively used for the investigation of the block end-to-end vector relaxation in PS−PI diblock copolymers[21−24] from the well-disordered to the ordered state; the dipole moment component along the PI backbone (Figure 1a) allows for the dielectric examination of the fluctuation of the end-to-end vector **R** of the PI block (Figure 2a). The situation is different for PS−PI−PS triblock copolymers having the PI block at the middle. For this midblock without a dipole inversion, the end-to-end vector will not fluctuate for either loops or bridges if the ends are fixed (to the "glassy" PS domains, because the measurements are usually done below the PS glass transition), and thus, the global midblock motion is not dielectrically active.[25] However, when a dipole inversion is introduced along the PI midblock (see Figure 1b), the total polarization is proportional to the vector $\Delta\mathbf{R} = \mathbf{R}_1 + \mathbf{R}_2$, where $\mathbf{R}_1$ and $\mathbf{R}_2$ are the midblock end-to-midpoint vectors (Figure 1b), and therefore, the global midblock motion can be detected for both loops and bridges (Figure 2b,c). Watanabe[19] used this concept and compared the low-frequency dielectric data of the triblock to those of the respective diblock, both forming ordered lamellae; by assuming that the relaxation function at low frequencies is dominated by that of loops (which is considered slower than that for bridges and similar to that for the tails in a diblock), the bridge fraction $\phi_{\text{bridge}} \cong 0.40$ was obtained, in the same range with theoretical estimates; large-amplitude oscillatory shear reduced this fraction to $\phi_{\text{bridge}} \cong 0.30$. More recently, Watanabe et al.[26] utilized an asymmetric triblock with similarly inverted dipoles along the middle PI block to demonstrate the importance of loops and bridges on the elasticity and plasticity of triblock copolymer solutions in solvents selective for the midblock. To analyze the dielectric data and extract ϕ_{bridge}, qualitative arguments on the entropic barriers determining the motion were used[19,26] to support the assumptions that the motion of bridges possesses an amplitude smaller than that of loops and that the relaxation function of the loops is similar to that of the tails in a diblock. Besides, the contribution of knotted loops or bridges (Figure 2d−f) to the dielectric loss was not considered.

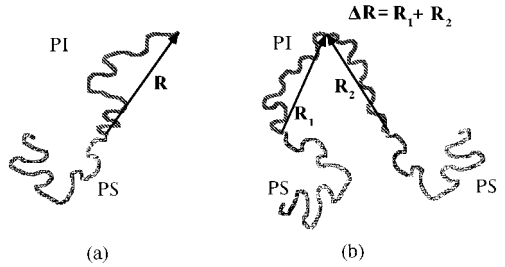

Figure 1. Schematic illustration of a PS−PI diblock copolymer and its dimer, a dipole-inverted PS−PI−PS triblock copolymer. The total along-the-chain dipole moment is proportional to the block end-to-end vector **R** for the diblock and to the vector $\Delta\mathbf{R} = \mathbf{R}_1 + \mathbf{R}_2$ for the triblock.

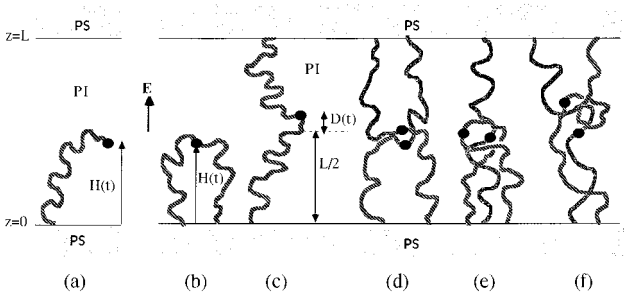

Figure 2. Schematic representation of PI block conformations in diblock and triblock copolymer lamellae. (a) Diblock lamella (tail). (b−f) Triblock lamella: (b) unknotted loop, (c) unknotted bridge, and (d−f) knotted loop/bridge. Dielectric relaxation reflects fluctuation of the free end of the tail or midpoint (dipole inversion point) of the loop/bridge (shown as the filled circle). **E** denotes the electric field parallel to the lamellae normal.

A question that remained open following Watanabe's work is what is a general and quantitative molecular picture for both loop and bridge relaxation. Besides, how the estimated values of the bridge fractions are affected by sample preparation or annealing, i.e., whether one can measure and discuss a real equilibrium bridge fraction, is left as an open question.

The present paper is an effort to extend Watanabe's work by investigating the effects of the sample preparation/annealing method on the dielectric relaxation behavior of triblock copolymers with symmetrically inverted dipoles along the chain backbone of the midblock. By comparing the observed behavior with that of the respective diblock, it is found that the emerging picture is more complicated than originally considered; i.e., the separation of the loops and bridges contributions to the observed dielectric relaxation is significantly affected by the sample history. It is proposed that annealing may affect not only the loop fraction but also the population of knotted loops and bridges (Figure 2d−f). At the same time, Monte Carlo computer simulations using the Cooperative Motion Algorithm (CMA) were employed to investigate the statics and dynamics of symmetric triblocks of different molecular weights. The results were compared with those for the respective diblocks. Investigation of the static structure revealed the transition to the ordered state at $\chi_{eff}N \cong 20$ (close to the literature values[11]) where a lamellar microdomain structure was formed. By identifying all of the individual midblock chains as either loops or bridges, the bridge fraction was evaluated in the range 0.50−0.37 for $N = 20-60$ (the estimations are made at $\chi_{eff}N \cong 100$), in agreement with the data. The investigation of the midblock dynamics by evaluating the orientational relaxation of the vector $\Delta\mathbf{R}$ individually for loops and bridges revealed that, at (a hypothetical) equilibrium where both end- and midblocks possess the same mobilities, the contribution of the intensity of loops is almost twice that of bridges, with both, however, having similar relaxation rates. The total intensity is much larger than that for the respective diblocks, which agrees with the data for the annealed triblock lamellae but not for the melt-prepared one. However, the dynamics of $\Delta\mathbf{R}$ of the triblock is found very similar to that of $\mathbf{R}$ of the diblock, which disagrees with the experiment for the annealed systems. In the actual experimental systems, the ends of the midblock PI chains are more-or-less fixed onto the glassy PS domains, whereas in the simulated systems, the ends of the midblock chains can fluctuate rather freely. This fact, probably resulting in the difference between the data and the simulation, in turn suggests the importance of the block junction mobility on block copolymer dynamics. Moreover, annealing may also affect the degree of "interdigitation" of loops and bridges in the experimental systems.

This article is arranged as follows: following the Experimental Section (II), the results of the dielectric relaxation investigations are presented in section III. The Monte Carlo computer simulations are presented in section IV and are discussed in relation to the data. Finally, the concluding remarks constitute section V.

II. Experimental Section

Materials. A poly(styrene-*b*-1,4-isoprene-*b*-styrene), PS−PI−PS, triblock copolymer having symmetrically inverted dipoles along the chain backbone of the midblock PI block, PS−$\overrightarrow{\text{PI}}$−$\overleftarrow{\text{PI}}$−PS, was synthesized[19] using a *p*-xylylene dichloride coupling reaction. First, PS−$\overrightarrow{\text{PI}}^{-}\text{Li}^{+}$ diblock anions were polymerized using *sec*-butyllithium in benzene. The resulting high-*cis*-PI block has type-A dipoles[20] aligned in the same direction. A fraction of the PS−$\overrightarrow{\text{PI}}$ diblock copolymer was recovered as a prepolymer, and the remaining anions were coupled with a prescribed amount of *p*-xylylene dichloride (≅95% equimolar to the anions) to produce symmetrical PS−$\overrightarrow{\text{PI}}$−$\overleftarrow{\text{PI}}$−PS triblocks with dipole inversion at the midpoint of the PI block. Finally, the small amount of the unreacted prepolymer was thoroughly removed by repeated fractionation from benzene/methanol mixtures to obtain a monodisperse PS−$\overrightarrow{\text{PI}}$−$\overleftarrow{\text{PI}}$−PS copolymer sample.

Table 1. Molecular Characteristics of the Samples

sample	M_{PS}	M_{PI}	w_{PS}[a]	M_w/M_n	N[b]	f_{PS}[c]	χN (25 °C)
SI(12−12)	11 700	11 600	0.50	1.04	277	0.47	45[d]
$SI(12-12)_2$	23 400[e]	23 200	0.50	1.05	554	0.47	90[d]

[a] Weight fraction of polystyrene (PS). [b] On the basis of average segmental volume. [c] Volume fraction of PS. [d] On the basis of $\chi = 0.05 + 34/T$. [e] Total molecular weight for the two PS blocks: each PS block has $M = 11\,700$.

Table 2. Preparation/Annealing History of the Triblock Samples

sample	preparation	annealing (days)
Melt-0	from-the-melt	0
Cast-A	slow casting	4
Cast-B1[a]	slow casting	6
Cast-B2[a]	slow casting	8
Cast-C	slow casting	10

[a] They refer to the same specimen.

The PS−$\overrightarrow{\text{PI}}$ and PS−$\overrightarrow{\text{PI}}$−$\overleftarrow{\text{PI}}$−PS copolymers were characterized with gel permeation chromatography (GPC) with a refractive index monitor and a UV absorption detector.[19] The elution solvent was THF, and commercially available monodisperse polystyrenes were used as elution standards. The macromolecular characteristics of both the PS−PI, identified as SI(12−12), and the PS−PI−PS, identified as $SI(12-12)_2$, samples are shown in Table 1. Note that the molecular microstructure of the SI(12−12) is identical to that of a half-contour of the $SI(12-12)_2$ copolymer.

Sample Preparation. Because one aim of this work is to understand the effects of sample preparation and annealing on the dielectric response, specimens for the dielectric measurements were prepared in different ways: For the specimens called prepared "from-the-melt", the material freeze-dried from a benzene solution was placed between the two electrodes under vacuum and pressure was applied to the electrodes at 100 °C for 5−6 h, to spread the polymer uniformly on the electrodes. For the solvent cast and annealed specimens, the material was dissolved in toluene (a solvent almost equally good for the two components) and slowly cast on the electrode under weak vacuum at a temperature close to the boiling point of the solvent. The samples were then annealed at 120 °C under vacuum for various times as shown in Table 2. In all cases, the solvent has been totally removed in the first stage, as evidenced from measurements of the local segmental dynamics (section III below).

The PS/PI lamellae prepared with the above methods are believed to be essentially parallel to the electrodes: With the slow solvent casting followed by annealing (the second method), the lamellar surface is known to become parallel to the surface of the casting solution,

i.e., to the substrate used as the electrode. With the first method, the applied pressure squeezed the freeze-dried material down to 50 μm thickness, and this squeezing flow possibly resulted in the lamellae parallel to the electrode (as suggested also from coincidence of the dielectric data explained later for Figure 4a).

Dielectric Measurements. Dielectric relaxation spectroscopy was used to investigate the collective chain dynamics of the PI blocks of the diblock and the triblock copolymers in the ordered state. Advantage is taken of the finite component of the dipole moment parallel to the PI chain backbone.[20] For macroscopic systems, dielectric relaxation reflects fluctuations of the total polarization in the direction of the applied electric field **E** (this direction is chosen as the *z*-direction throughout this paper). The corresponding relaxation function is given by the autocorrelation function of the *z*-component of the polarization, $P_z(t)$,[27]

$$C(t) = \langle P_z(t)P_z(0)\rangle \tag{1}$$

where, for convenience of the discussion later, the relaxation function is not normalized. The complex dielectric permittivity, $\epsilon^*(\omega) = \epsilon'(\omega) - i\epsilon''(\omega)$ ($i = (-1)^{1/2}$), the quantity measured in this study, is given by the one-sided Fourier transform of the time derivative of this $C(t)$,[27]

$$\epsilon^*(\omega) = \epsilon_\infty - K\int_0^\infty \frac{\mathrm{d}C(t)}{\mathrm{d}t} e^{-i\omega t}\,\mathrm{d}t \tag{2}$$

where ϵ_∞ is the high-frequency dielectric constant and K is a numerical constant proportional to F/k_BT, with k_B, T, and F being the Boltzmann constant, absolute temperature, and a correction factor accounting for a difference of the internal (local) and macroscopic electric fields, respectively.

The relaxation mode distribution of $\Delta C(t) = C(t) - C(\infty)$ is reflected in the dielectric dispersion, i.e., in the dependence of ϵ'' on the angular frequency ω. If the mode distribution of $\Delta C(t)$ is described by a spectrum $\tilde{F}(\ln\tau)/K$, then

$$\Delta C(t) = \frac{1}{K}\int_{-\infty}^{\infty} \tilde{F}(\ln\tau)\exp[-t/\tau]\,\mathrm{d}(\ln\tau) \tag{3}$$

and ϵ'' is represented as a superposition of Debye processes,

$$\epsilon''(\omega) = \int_{-\infty}^{\infty} \tilde{F}(\ln\tau)\frac{\omega\tau}{1+(\omega\tau)^2}\,\mathrm{d}(\ln\tau) \tag{4}$$

A proportionality between ϵ'' and ω (the terminal behavior) is observed at frequencies well below $1/\tau_1$, with τ_1 being the longest relaxation time (i.e., $\tilde{F}(\ln\tau) \to 0$ for $\tau \gg \tau_1$). Consequently, if $\tilde{F}$ does not vanish at τ, the weaker ω dependence is seen at corresponding frequencies, $\omega \cong 1/\tau$; specifically, a power-law behavior, $\epsilon'' \propto \omega^a$ ($0 < a < 1$), is observed if $\tilde{F}$ exhibits a power-law decay, $\tilde{F} \propto \tau^{-a}$. The dielectric relaxation intensity, $\Delta\epsilon = \epsilon'(0) - \epsilon'(\infty) = (2/\pi)\int_{-\infty}^{\infty}\epsilon''(\omega)\,\mathrm{d}(\ln\omega)$, is related to $\Delta C(0)$ as

$$\Delta\epsilon = K\Delta C(0) = \int_{-\infty}^{\infty}\tilde{F}(\ln\tau)\,\mathrm{d}(\ln\tau) \tag{5}$$

This $\Delta\epsilon$ as well as the relaxation mode distribution of $\Delta C(t)$, i.e., the ω dependence of ϵ'', are utilized in the arguments for the dielectric behavior of the di- and triblock copolymer lamellae. For multiple relaxation processes, the dielectric strength of each one is evaluated by integrating $\tilde{F}(\ln\tau)$ over the appropriate range of τ.

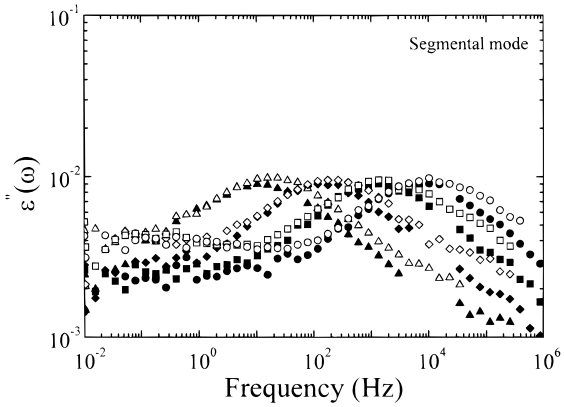

Figure 3. Frequency dependence of the dielectric loss $\epsilon''(\omega)$ for the SI(12−12)$_2$ ordered triblock copolymer (solid symbols) and for the SI(12−12) ordered diblock (open symbols) in the temperature range where the polyisoprene segmental motion is observed for various temperatures: (▲,△) 223, (◆,◇) 229, (■,□) 235, and (●,○) 241 K.

The spectrum of relaxation times $\tilde{F}(\ln\tau)$ is evaluated by a direct transformation of the dielectric $\epsilon''(\omega)$ data (eq 4) with a recently proposed method,[23] which is based on a modification of the widely used CONTIN routine[28] for the analysis of photon correlation spectroscopy[29] data; the significant advantage of the routine is that it provides reliable statistical criteria for the support or rejection of the nominally proposed solutions. Similar analyses, on the basis of integral inversion, have been proposed by others[30,31] as well.

A framework of the dielectric spectroscopy relevant to this work is presented in Appendix A with emphasis on the relationship of the dielectric loss to the relaxation function of vector **R** of the diblock and that of vector Δ**R** of the triblocks.

The dielectric measurements were performed with a Solatron-Schlumberger frequency response analyzer FRA 1260, supplemented by using a high-impedance preamplifier of variable gain, covering the frequency range 10^{-2}−10^6 Hz. The sample was residing between two gold-plated stainless steel electrodes (diameter 25 mm) with a spacing of 50 ± 1 μm maintained by two fused silica fibers 50 μm in diameter; attention is paid to achieve a good contact between the sample and the electrodes. The sample was kept in a cryostat with its temperature controlled via a high-pressure nitrogen gas jet heating system with a Novocontrol Quatro controller, allowing a stability of the sample temperature in margins of ±0.1 °C in a broad temperature range of −160 to +300 °C (in the present system, the temperature range covered was −70 to +300 °C). The absolute values of the loss part of the dielectric permittivity, ϵ'', depend on the accuracy of the value of the sample thickness provided to the instrument software.

III. Experimental Results and Discussion

1. From-the-Melt Samples without Annealing. *Overview.* Figure 3 shows a semilog plot of the loss part of the dielectric permittivity, $\epsilon''(\omega)$, versus frequency for the "melt-prepared" symmetric ordered triblock copolymer SI(12−12)$_2$ in the temperature range corresponding to the polyisoprene segmental mode (223−241 K) together with the data for the SI(12−12) diblock. The two

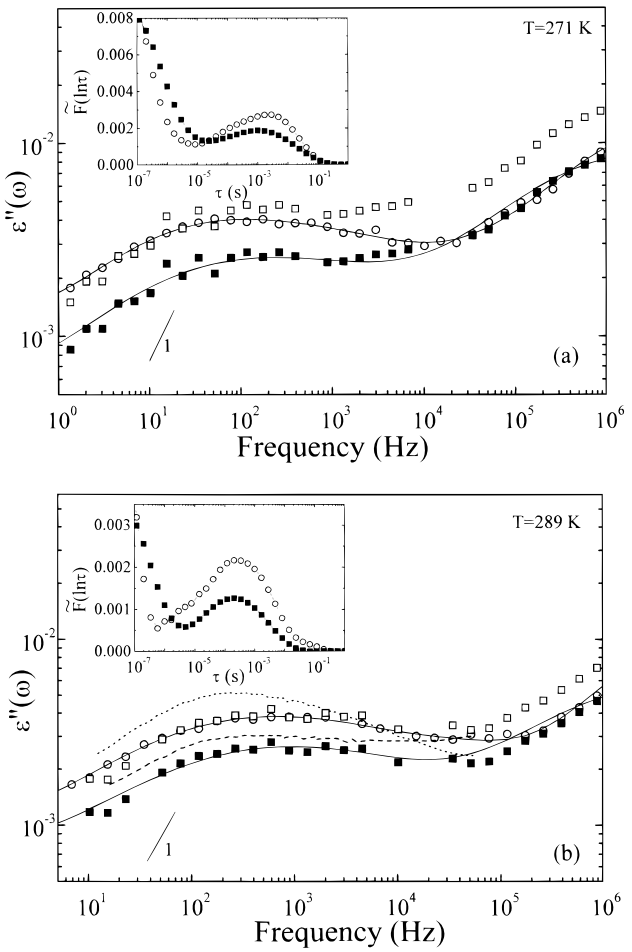

Figure 4. Comparison of the dielectric loss data between the SI(12−12) diblock (○) and the SI(12−12)$_2$ triblock (■) at (a) 271 K and (b) 289 K. The solid lines through the data points are the fits (eq 4) in order to extract the relaxation spectra (distribution of relaxation times), $\tilde{F}(\ln \tau)$, in the respective insets. The open squares (□) indicate the shifted loss data of the triblock, $\lambda\epsilon''_{\text{triblock}}$, with the shift factor λ being chosen to achieve the best superposition on the $\epsilon''_{\text{triblock}}$ data of the diblock at low frequencies, $f < 10^2$ Hz at 271 K and $f < 10^3$ Hz at 289 K. The dotted and dashed lines in part b are dielectric loss data for SI(12−12) (.....) and SI(12−12)$_2$ (- - - - -) at 289 K from Watanabe[19] (see text).

sets of data agree with each other at all temperatures in this range (the small differences in the low-frequency range are due to the chain motion contribution discussed below), verifying that in this dynamic regime there is no significant additional contribution from a different relaxation process in the triblock relative to the diblock. It also verifies that on the scale of the local segmental motion there is no difference between the ordered tri- and diblock copolymers (see Figure 5 below). Actually, this segmental motion is similar to that of a PI homopolymer of the same molecular weight, in agreement with previous studies[24] in the ordered state.

As the temperature increases, another relaxation process enters our frequency window. Figure 4 shows the dielectric loss data of the triblock lamella in comparison with the data for the diblock at two temperatures where the normal mode relaxation is observed in our frequency window: (a) 271 and (b) 289 K. The solid curves through the data points are the fits (eq 4) to the $\epsilon''(\omega)$ data in order to determine the relaxation spectra $\tilde{F}(\ln \tau)$, shown in the insets. The open squares in Figure 4 are the triblock data multiplied by a factor

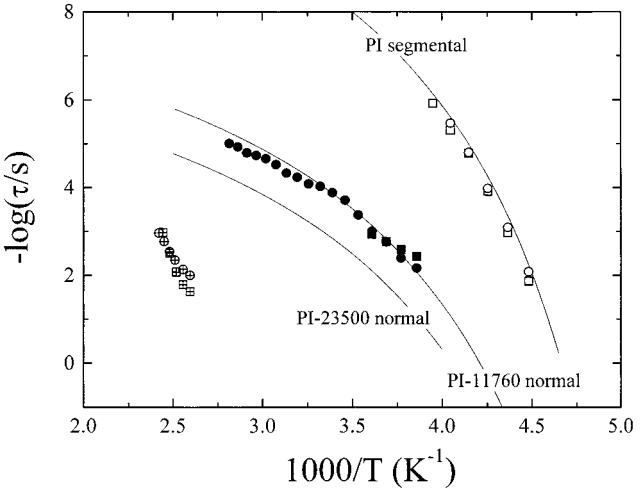

Figure 5. Arrhenius plot of the temperature dependence of the most probable relaxation times of the fast segmental process (○, □), the intermediate chain motion (●, ■), and the slow interface-related process (⊕, ⊞) obtained from the peak location of the corresponding relaxation spectra $\tilde{F}(\ln \tau)$ for the SI(12−12) ordered diblock (○, ■, ⊕) and the melt-prepared SI-(12−12)$_2$ ordered triblock copolymer (□, ■, ⊞). Lines denote the segmental and normal mode relaxation times of homopolymer polyisoprene of molecular weights 11 760 and 23 500 from earlier works.[32,33]

λ, $\lambda\epsilon''_{\text{triblock}}$, with $\lambda = 1.76$ (at 271 K) and 1.51 (289 K). A very important characteristic of this process is that, within the error, it exhibits the same dynamics as that of the PI block of the diblock over the whole temperature range where the process is within the window of the technique (in agreement with the earlier data[19] at 313 K). This is shown in Figure 5, which depicts the temperature dependence of the most probable (not the longest) relaxation times τ_{peak} obtained from the peak location of the spectra $\tilde{F}(\ln \tau)$ for both the di- and triblock samples; these τ_{peak} values are also in agreement with the normal mode process of a PI homopolymer of molecular weight 11760 (shown in Figure 5 with a solid line based on previous data[32,33]). The agreement regarding the segmental PI relaxation between the diblock and the triblock as well as with the above homopolymer is also evident.

In Figure 5, the relaxation times are also shown for a third, slower process (observed at $T \geq 400$ K), which has been observed before for ordered diblocks[21,24] (with amplitude that depends on the sample preparation) and was apparently related to the coherently ordered microstructure; it was attributed[24] to the relaxation of the conformal interfaces formed in the ordered state, and this assignment was in harmony with computer simulation.[34] The relaxation times of this process were independent of sample preparation, and the simulations suggested[34] that the times depended on the period of the lamellae; the observed relaxation times are the same for the tri- and diblock samples, possibly due to the equivalent lamellar spacing.

The dotted and dashed curves in Figure 4b are the previous data[19] of the di- and triblock lamellae reduced at 289 K. In that study, the di- and triblock lamellae were prepared directly on the electrode via slow solvent casting from toluene (for 1 week at ∼303 K) and successive vacuum-drying for a week at ∼343 K (lower than the glass-transition temperature of the PS block of molecular weight 11 700; $T_g^{\text{PS}} \cong 367$ K). This preparation resulted in an alignment of the lamellae almost parallel to the electrodes, as observed by transmission

electron microscopy.[19] In contrast, the present from-the-melt lamellar specimens were prepared from the freeze-dried copolymer materials by essentially compression molding at ~373 K ($> T_g^{PS}$) for 5−6 h. This molding (down to the specimen thickness of 50 μm) resulted in a rather strong squeezing flow, which should induce a certain alignment of the lamellae parallel to the electrodes. Although the domain orientation in the present specimens was not experimentally examined and, thus, is not known, the similarity of the present dielectric data to those of Watanabe[19] (Figure 4b) is a strong indication of a similar morphology/orientation; i.e., it is believed that the present treatment of the from-the-melt specimens was capable of orienting the microdomains parallel to the electrodes, and thus, the dielectric behavior of the from-the-melt specimens can be discussed on the basis of the dielectric formulations for a lamella subjected to the electric field in the direction of its normal (Appendix A).

In Figure 4, the terminal relaxation behavior characterized by the proportionality between ϵ'' and frequency is observed neither for the diblock nor for the triblock lamellae. Instead, the data exhibit power-law-like tails at low frequencies, $\epsilon'' \propto f^a$ with $a \cong 0.3$. The corresponding power-law behavior, $\tilde{F} \propto \tau^{-a}$ for large τ, was noted for the relaxation spectrum, although this behavior is not clearly demonstrated in the semilogarithmic plots shown in the insets. These results indicate that the global relaxation of the PI blocks in these lamellae is significantly broadened and retarded as compared to the relaxation of homo-PI chains.[21,35] The retardation and broadening are essentially attributed to the thermodynamic requirement of preserving uniform density discussed in Appendix A.

Estimation of Unknotted Bridge Fraction. An attempt is now made to estimate the fraction of unknotted bridges, ϕ_{bridge}, from the ϵ'' data of the di- and triblock lamellae. The PI blocks in the diblock lamellae have the tail conformation, whereas those in the triblock lamella have the loop and bridge conformations (Figure 2). The previous arguments[19,26] suggest that the dielectric relaxation behavior is similar for the tails and unknotted loops, whereas the relaxation is faster and its intensity is smaller for the unknotted bridges. If it is assumed that the knotted loops/bridges do not significantly contribute to the ϵ'' data of the triblock, this argument allows one to estimate ϕ_{bridge} from the data of the di- and triblock lamellae, as explained in Appendix A.

The good superposition of the $\epsilon''_{diblock}$, and the shifted $\lambda\epsilon''_{triblock}$ data at low frequencies (see open circles and squares in Figure 4), indicates that the distribution of *slow* relaxation modes is similar for the two lamellae but their intensity is smaller for the triblock. This coincidence of the slow mode distribution is in harmony with the above argument,[19,26] suggesting no significant contribution of the knotted chains to $\epsilon''_{triblock}$. Then, one may estimate ϕ_{bridge} on the basis of eq A15,

$$\phi_{bridge} = (\lambda - 1)/\lambda = 0.43 \pm 0.01 \quad \text{(at 271 K)}$$
$$0.34 \pm 0.02 \quad \text{(at 289 K)}$$
$$\text{from-the-melt lamellae} \qquad (6)$$

where λ (=1.76 ± 0.02 at 271 K and 1.51 ± 0.02 at 289 K) is the shift factor that gave the best superposition of the $\epsilon''_{triblock}$ and $\epsilon''_{diblock}$ data. (λ^{-1} is the unknotted loop fraction in the above argument.) Alternatively, one may estimate ϕ_{bridge} utilizing the ratios of the dielectric intensities $\Delta\epsilon_n$ for the normal mode relaxation, which were evaluated by integrating the spectrum $\tilde{F}(\ln \tau)$ in the insets over the appropriate range of τ. Averaging over the temperatures investigated results in

$$\Delta\epsilon_{n,triblock}/\Delta\epsilon_{n,diblock} = 0.60 \pm 0.05 \qquad (7)$$

If the dielectric intensity of the unknotted bridges is significantly smaller than that of the unknotted loops, one may utilize this ratio in eq A16 to estimate ϕ_{bridge}. The results were

$$\phi_{bridge} = 0.40 \pm 0.05 \quad \text{from-the-melt lamellae} \qquad (8)$$

The ϕ_{bridge} values estimated with the two different methods are reasonably close, suggesting that the $\Delta\epsilon_n$ is actually smaller for the unknotted bridges than for the unknotted loops. Note, however, that both methods involve certain assumptions and the estimated values should be considered with caution. Besides, the differences in the mode distribution should probably be attributed to the bridge relaxation, which signifies that the bridges have a small but nonnegligible contribution to $\Delta\epsilon_n$.

The ϕ_{bridge} values of the from-the-melt triblock lamellae (eqs 6 and 8) are reasonably close to the value for the previously studied solvent-cast lamellae, $\phi_{bridge} = 0.41$ ($\lambda = 1.7$)[19] and in the same range with theoretical estimates[6,7,14−16] of $\phi_{bridge} \cong 0.4-0.46$ in the limit of strong segregation; in the present case and in the temperature range ($T \leq 289$K) where the chain motion is observed, the effective χN is about 90, and the triblock resides in strong segregation.[36] Thus, in these lamellae prepared with different methods, the distribution of the PI block conformations does not seem to be significantly different, and the dielectric method (eqs A15 and A16) seems to be useful in estimating ϕ_{bridge} of the unknotted chains.

At this point, one should again note the limitations of this dielectric method together with its usefulness. First, the method is based on a molecular argument, and one should not overestimate the accuracy of the resulting ϕ_{bridge} values; actually, it was suggested[19] that the ϕ_{bridge} value free from this argument can be dielectrically obtained if the ϵ'' of a model system composed of triblocks and ring-diblocks is compared with ϵ'' of the triblock. Second, the molecular argument does not incorporate the effect of spatial confinement[35] on the dielectric behavior of the PI blocks analyzed in Appendix B; incorporation of this effect might result in a somewhat larger ϕ_{bridge} value. As judged from Table 6 in Appendix B, the dielectric intensity may be somewhat larger for the loops than for the tails and eq 15 should be modified as $\epsilon''_{PS-PI-PS}(\omega) \cong r\phi_{u.loop}\epsilon''_{PS-PI}(\omega)$, with r being a number slightly larger than unity. A much more severe third limitation of the dielectric evaluation of ϕ_{bridge} is related to the contribution of knotted chains (cf. Figure 2). The dynamic behavior of these chains is not fully incorporated in the argument for eqs A15 and 16. In addition, the behavior of the knotted loops and knotted bridges would not be significantly different, and it becomes difficult (and conceptually useless) to dielectrically distinguish these chains. Because the triblock lamellae would contain a nonnegligible amount of the knotted chains at the *real* equilibrium where the motion of the PS−PI junctions is not frozen, one may have to

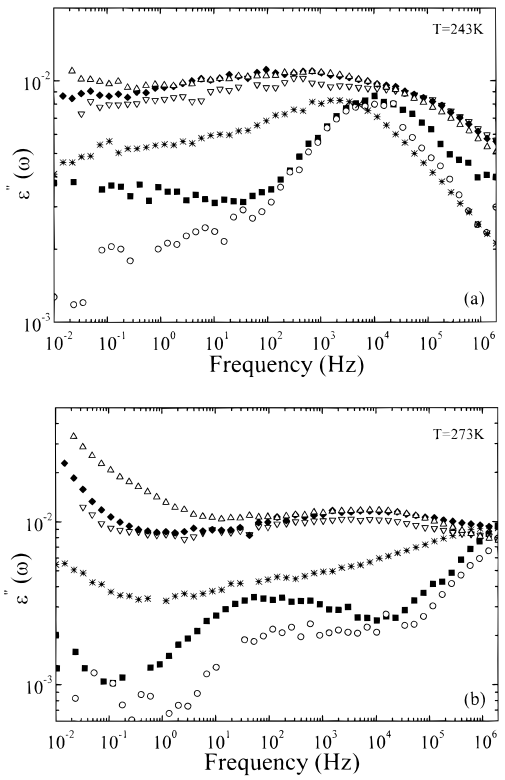

Figure 6. Effect of the sample preparation method and annealing on the dielectric loss data at (a) low temperature (243 K) where the polyisoprene-block segmental relaxation is observed and (b) higher temperature (273 K) where the polyisoprene-block normal mode is measured. Different symbols denote the diblock (○) and various triblock samples: (■) from-the-melt, (*) Cast-A, (▽) Cast-B1, (◆) Cast-B2, and (△) Cast-C.

limit the dielectric estimation of ϕ_{bridge} with the present methodology (eqs. A15 and A16) only to a *partial* equilibrium state where the number of the knotted chains is considerably smaller than that at the real equilibrium and the PS−PI junction motion is frozen to suppress an increase of this amount. The present from-the-melt lamellae as well as the solvent-cast lamellae of Watanabe[19] seem to be in this partial equilibrium state.[37] For these lamellae, the dielectric method works to give the estimate of ϕ_{bridge} in the actual specimens (not in the real equilibrium).

2. Samples Prepared with Solvent Casting and Annealing. The effect of the sample equilibration on the dynamics of the midblock chains was investigated using the series of samples prepared with slow solvent casting at high temperature (close to the boiling point of toluene) followed by annealing at 393 K ($> T_g^{PS}$) for various times (Table 2). Slow solvent casting is well-known to produce a more coherent microdomain structure[3,38,39] and to allow the system more time to attain thermodynamic equilibrium.[40,41] It is expected that this will influence the possible chain conformations,[42] i.e., the population distribution of the knotted/unknotted loops and bridges for the triblock lamellae.

Figure 6 shows the effect of sample preparation and annealing time on the $\epsilon''(\omega)$ data of the triblock. Figure 6a shows the data for a temperature where the PI segmental motion is detected, whereas Figure 6b shows the data for a temperature where the global chain motion is observed. Also shown are the data (at the same temperatures) for a from-the-melt triblock sample and for the diblock. A significant increase is evident on the low-frequency side of the segmental relaxation in the data of the "Cast-A" specimen as compared with that of the from-the-melt one, indicating the existence of a relaxation process with a very broad mode distribution (almost 3 decades), which is slower than the segmental relaxation but essentially faster than the normal mode of the tail PI blocks of the diblock and the one observed for the from-the-melt specimen (discussed before). These differences become even more pronounced with increasing annealing time (data of "Cast-B1", "-B2", and "-C" specimens). Moreover, the data for Cast-B2 and -C are very similar (except for a difference at very low frequencies in Figure 6b due to the contribution of conductivity), indicating that the sample prepared by slow casting reaches equilibrium within 8 days annealing at 393 K (Cast-B2). This was also verified with subsequent measurements on specimen Cast-C annealed for an extra week. The significant enhancement of the dielectric loss intensity in the frequency range between the segmental motion and the motion of the PI tails of the diblock, observed in Figure 6 for specimens Cast-B1, -B2, and -C, indicates a highly correlated motion of the chains that relax with this particular dynamic process (called "LB" from now on). Note that the segmental motion, although partially overlapping with the LB process, is clearly identified at low temperatures/high frequencies (Figure 6a).

For sample Cast-A, where the conductivity contribution appears at higher temperatures, the slow process related to the correlated motion of the interfaces in the lamellar-ordered copolymers[24] is also observed (not shown). For the other specimens, the segmental process and the process LB are observed, whereas the interfacial process is hidden behind the increased conductivity contribution, which appears at lower temperatures than for Cast-A.

In the LB relaxation domain (Figure 6b), the ϵ'' of the annealed triblock lamellae depends very weakly on frequency without a significant loss peak, and thus, the relaxation mode distribution is very broad. Such a broad distribution may be exclusively attributed to an extra cross-correlation (or coupling[43]) of the relaxation of midblocks in the triblock lamellae that has emerged during annealing. For the diblock lamellae annealed in a similar manner, neither any appreciable broadening of the mode distribution nor any enhancement of the magnitude of ϵ'' was observed. Therefore, the broadening and the intensity enhancement observed for the annealed triblock can be attributed to conformational changes exclusively occurring for the midblocks of the triblock lamellae. This conformational change might be the formation of knotted (interdigitated) configurations[26] on annealing. For the midblocks *spatially confined* in a lamella, it was suggested[35] that the knot formation enhances the cross-correlation of chains leading to an increase of the dielectric intensity; those results are summarized in Appendix B. A possibility was also noted that a similar increase of the intensity may occur due to the knot formation for the chains that are subjected to the thermodynamic requirement of preserving uniform density, which is the essential factor that broadens and retards the block relaxation as compared to homopolymer chains.

In the dielectric spectroscopy literature, such significant increases in dielectric strength have been attributed to the contribution of the Kirkwood correlation

factor,[44] h, due to extra correlations between a certain dipole and its neighbors,[45] which introduces a factor h in the calculation of the average of the system polarization $\langle \mathbf{P}^2 \rangle = h\mathbf{P}^2$. The Kirkwood factor h is given by $h = 1 + \sum_{i,j} \overline{\cos \phi_{ij}}$, where indices i and j are over all chains and ϕ_{ij} is the angle between a reference chain i and a chain j; if each of the z near-neighboring chains contributes equally to cos ϕ, then $h = 1 + z\overline{\cos\phi}$. It has been reported[46] that h can take values even much larger than 1, and therefore, this can explain the increased value of the dielectric strength. This mutual enhancement of polarization in the present case may be due to the formation of knotted configurations in the annealed triblocks. Moreover, it is obvious that the correlation factor h is unity (i.e., $\overline{\cos\phi} = 0$) in the case that the dipole moment vectors $\mathbf{P}$ can individually assume any random orientation, as in the case of the tails in the diblock and as was assumed for the motion of the triblock midblocks for the from-the-melt prepared specimens. It should be noted that application of the Kirkwood−Fröhlich[44,47] theory indirectly assumes that the "units of polarization" (here the midblock chains) remain discrete units, so as to retain the "memory" of orientation; i.e., they are not in a state where the identity of each individual chain is lost, for example, in a strongly entangled regime. This is true in the present case because the molecular weight of the midblock PI chain is only about two times larger than the characteristic molecular weight[48] where entanglement effects influence the chain dynamics.[33]

Comparing the behavior of the fully annealed triblock (Cast-C) and the from-the-melt diblock, the latter containing only the tail-type PI blocks, by calculating the dielectric strength (using the distribution of relaxation times analysis) for temperatures where the LB process relaxes inside the experimental frequency window (261−287 K) results in $\Delta\epsilon_{n,\text{triblock}}/\Delta\epsilon_{n,\text{diblock}} \cong 2$. Interestingly, this ratio is fairly close to the factor of 10/4 (see Table 6 in Appendix B), expected from a model calculation[35] for the tail and the fully knotted loops/bridges (modeled as a bundle of tails) both subjected to spatial confinement but in the absence of the density preserving requirement. In the presence of this requirement, the dielectric intensity of the knotted chains may be somewhat increased as compared to that in the model calculation, possibly resulting in the observed difference between the above two lamellae. Thus, it is conceivable that the knot formation can result in the observed effect of annealing: in the presence of both the confinement and the density-preserving requirement, the knot formation would not only increase the dielectric intensity but also broaden the mode distribution (due to enhanced cross-correlations).

Concerning this point, one has to remember that the from-the-melt specimen was prepared via compression-molding of a material freeze-dried from a benzene solution. During this freeze-drying procedure, the triblock chain configuration should have been frozen at some concentration where the microphase separation occurred but the chains were not fully knotted. This frozen configuration would be essentially preserved during the compression-molding (or, the squeezing flow on molding might have even decreased the knot content). Thus, annealing at 393 K ($> T_g^{\text{PS}}$) could increase the knot content to an equilibrium content at 393 K to induce the enhancement/broadening of the dielectric relaxation of the triblock lamellae. In this context, it is expected that the fully annealed specimens retained this knot content at 393 K even after they were cooled to the experimental temperatures ($\leq$273K).

The dynamic behavior of the knotted chains is not fully incorporated in the argument for eqs A15 and A16, whereas the behavior of the knotted loops and knotted bridges would not be significantly different so that the dielectric distinction of these knotted chains is difficult (and conceptually useless). For these reasons, it is not (and probably should not be) attempted to estimate the fractions of the knotted bridges/loops in the annealed triblock lamellae. Moreover, one has to remember that the ϕ_{bridge} for the unknotted bridges can be dielectrically estimated for the from-the-melt triblock lamellae because of the quenched chain configuration therein. A similar situation is noted for the specimens of Watanabe[19] prepared via slow solvent cast at 303 K followed by vacuum-drying/annealing at 343 K, with these temperatures being substantially lower than T_g^{PS}.

Finally, a brief statement is added about the effect of concentration on the knot formation. Watanabe et al.[26] examined the dielectric behavior of PS−PI−PS and PS−PI copolymers in a PI-selective solvent, *n*-tetradecane. The copolymer concentration was 50 wt %, and spherical domains of the PS blocks were formed in the solutions at low temperatures (where the PS blocks were not dissolved in *n*-tetradecane). Reversible changes of the dielectric data were found for both di- and triblock solutions in a range of temperature including that of the order−disorder transition. For those data representing the equilibrium behavior of the blocks, no enhancement/broadening of the triblock relaxation was observed on annealing. This difference between the solution and the bulk specimen (Cast-C in Figure 6b) may be partly related to a smaller knot content in the solution at equilibrium: swollen midblocks tethered on spherical PS domains would tend to take unknotted conformations. Thus, the ϕ_{bridge} value estimated from the ϵ'' data of the tri- and diblock solutions[26] may be the fraction for the unknotted bridges, although the previous study[26] did not rule out a possibility that ϕ_{bridge} estimated from the data at *intermediate* frequencies may include both unknotted and knotted bridges.

IV. Monte Carlo Computer Simulations

Computer simulations are employed utilizing the Cooperative Motion Algorithm[49,50] in order to probe the static and dynamic behavior of symmetric triblocks as a function of molecular weight and compare the behavior to that of the respective diblocks; the aim is to investigate the true equilibrium features of the morphology and the dynamics in these systems. A main difference between the experimental systems and the triblocks investigated by the simulation is the fact that equal mobilities are considered in the simulation for the two components forming the triblock. This means that, in the simulated systems, the ends of the midblock chains can fluctuate, restricted only by the thermodynamic potential in the ordered state, whereas those in the experimental specimens are more-or-less frozen at the interfaces with the glassy polystyrene.

The details of the simulation method have been presented before for the simulation of diblock copolymers[34] and are summarized in Appendix C. Four linear symmetric triblocks and their respective diblocks are considered; their characteristics are shown in Table 3.

Table 3. Characteristics of the Block Copolymers Simulated

notation	N_{total}	N_A[a]	N_{B_1}[a]	N_{B_2}[a]
BAB-20	20	10	5	5
BAB-30	30	14	8	8
BAB-60	60	30	15	15
BAB-90	90	44	23	23
AB-10	10	5	5	
AB-15	15	7	8	
AB-30	30	15	15	
AB-45	45	22	23	

[a] For the triblocks, B_1 and B_2 are the two end-blocks and *A* is the middle block. For the diblocks, A and B_1 are the two blocks (the A block of the diblock is equal to half of the A block of the triblock).

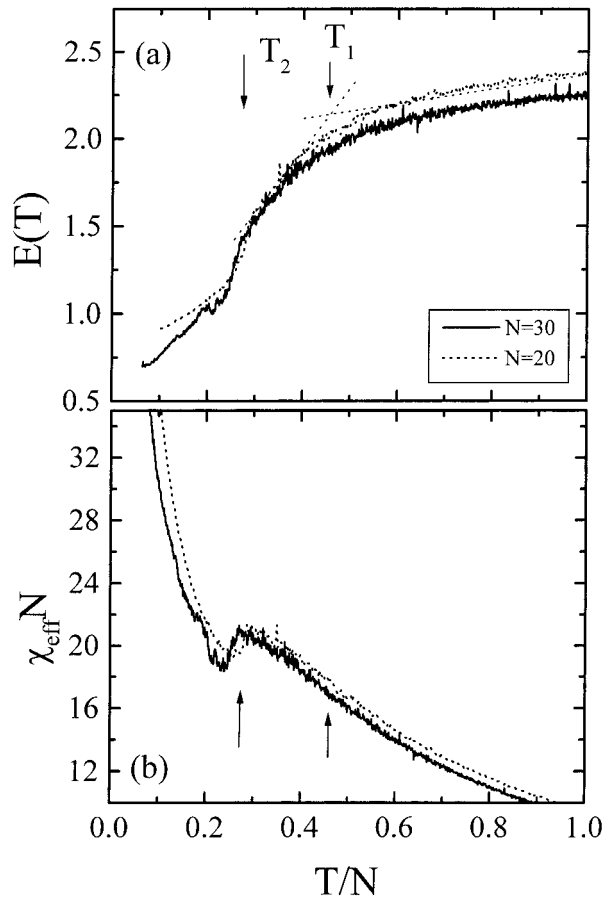

Figure 7. Temperature dependencies of various thermodynamic quantities determined for the Monte Carlo computer simulations of symmetric triblocks BAB-20 (dotted lines) and BAB-30 (solid lines) upon heating: (a) effective interaction energy per monomer $E(T)$ and (b) $\chi_{eff}N$ values, where χ_{eff} is the effective interaction parameter. The characteristic temperatures T_1 and T_2 are shown by arrows and are assigned according to the discussion in the text.

Static Properties. The thermodynamic properties of the simulated systems are analyzed first in order to determine the temperatures of phase transitions and characterize the related structure and the structural changes.

The microphase-separation temperature can be determined[34,51] from the temperature dependence of the energy of the system or of the energy fluctuations (which allow the determination of the specific heat). Figure 7a shows the energy of interaction per monomer (eq C1) as a function of reduced temperature (T/N) in a wide temperature range for two triblocks BAB-20 and BAB-30 upon heating; the resulting effective interaction parameters (eq C3) are shown in Figure 7b. It was proven that the heating rate was slow enough to give a rate-independent shape of the energy curve. For diblock copolymers,[34] two characteristic temperatures (T_1 and $T_2 = T_{ODT}$) were identified, at which the thermodynamic quantities changed in a specific way. Temperature T_1 was assigned to the broad crossover region where a broad step was observed in the specific heat from a very low value at high temperatures to a higher value below T_1. In the same temperature range, the effective interaction parameter began to deviate considerably from the $\chi_{eff} \propto 1/T$ dependence at high temperatures toward a plateau below T_1; T_1 was then assigned to indicate a crossover between a high-temperature homogeneous regime and a regime where concentration fluctuations begin to increase considerably with decreasing temperature. On the basis of the earlier findings and the behavior of the temperature dependence of the concentration fluctuations and the orientational correlations (not shown; see Figure 3 of Pakula et al.[34]), this temperature is also indicated in Figure 7 for the triblocks, although it is not clearly evident. This may be due to a different contribution of fluctuation effects in the case of triblocks[9] compared to diblocks[34] because the interactions of both end-blocks with the midblock are coupled.

At lower temperatures, a second characteristic temperature T_2 was assigned[34] to a stepwise change in the energy and a weak corresponding peak in the specific heat curve also supported by the calculations of the concentration fluctuations and the local and global orientational correlations; T_2 signifies the disorder-to-order transition temperature (ODT). In the triblock systems shown in Figure 7, a significant stepwise change in the energy is observed, and the ODT is assigned at $(T/N)_{ODT,BAB} \cong 0.25-0.27$. The respective ODT for the diblocks both in the present study and in the earlier one[34] is $(T/N)_{ODT,AB} \cong 0.46$; i.e., the transition to the ordered state occurs at a lower temperature for the triblock than for the respective diblock in agreement with theory[11] and experiment.[9,10] At the same time, the value of the product $\chi_{eff}N$ at the transition is found $(\chi_{eff}N)_{ODT,BAB} \cong 20$ in very good agreement with theory.[11] It is noted that no extra N dependence of $(\chi_{eff}N)_{ODT,BAB}$ was determined in the range of molecular weights simulated. The curves shown in Figure 7 were calculated on heating; the respective curves on cooling show a smaller step in the energy curve at the temperature T_2 signifying the ODT.

Figure 8a shows a projection of triblock BAB-60 in the disordered state ($T/N = 1$) on coordinates that are not subjected to the periodic boundary conditions; the homogeneous mixing of the blocks is evident. Figure 8b depicts the projection of the triblock BAB-60 on the lattice coordinates following cooling to $T/N = 0.05$, where a microphase-separated lamellar structure is observed. In this case as well as in the cases of BAB-20 and BAB-30, the lattice size ($30 \times 30 \times 30$) was such that the whole system simulated shows a monocrystalline region of the structure. For the BAB-90 triblock simulated on a much larger lattice ($60 \times 60 \times 60$), however, the cooling to the ordered state resulted in a polycrystalline lamellar structure (not shown) where two different lamellar orientations were observed with a more "homogeneous-like" structure in the vicinity of grain boundaries; this feature persisted even after long-time equilibration in the ordered state.

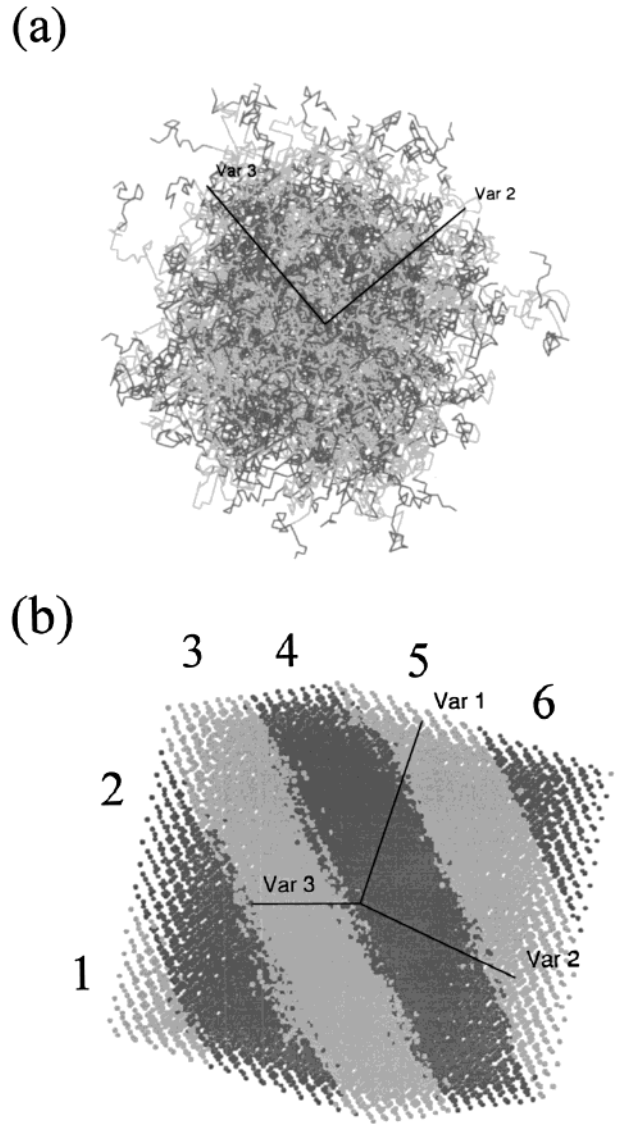

Figure 8. (a) Projection of a snapshot of the real space morphology of triblock BAB-60 in the disordered state at $T/N = 1$ on coordinates not subjected to the periodic boundary conditions. Different shadings represent the two types of monomers A and B. (b) Projection of a snapshot of the real space morphology of triblock BAB-60 on the lattice coordinates in the ordered state at $T/N = 0.05$. Different shadings represent the two types of monomers A and B, whereas the lines joining monomers belonging to the same chains are not drawn for clarity. Different numbers represent the successive lamellae determined with the algorithm discussed in the text.

The information on the structure was necessary in order to determine the bridge fraction of the midblock. Following the cooling of the system to the microphase-separated state and equilibration, a specifically developed algorithm was used to identify each individual A or B microdomain of the lamellar structure (numbers 1−6 in Figure 8b for BAB-60). Then, each individual chain was examined in order to determine whether its two end-blocks B_1 and B_2 reside at the same microdomain or at opposite ones separated by an A domain. In the former case, the midblock conformation is identified as a loop whereas in the latter as a bridge. Table 4 lists the bridge fraction ϕ_{bridge} determined for the three triblocks BAB-20, -30, and -60 (the polydomain structure of BAB-90 did not allow for the identification of each domain with the algorithm mentioned above and, thus, the determination of the bridge fraction). The ϕ_{bridge} values in Table 4 are indeed equilibrium values, as verified by extra equilibration of the systems in the ordered state when the obtained ϕ_{bridge} values essentially do not change. The estimated errors in the second column of Table 4 denote these small changes, which may be due to either an error introduced during the loop/bridge identification or an exchange of chains between the two conformations. It is also noted that the simulation for the BAB-30 on a different lattice ($30 \times 30 \times 40$) resulted in a value for ϕ_{bridge} (0.48), which is essentially within the error of the value in Table 4. Note that in the present simulations it was not computationally possible to separate unknotted from knotted chain configurations; thus, the ϕ_{bridge} values in Table 4 are the total for unknotted and (possibly) knotted bridges.

Table 4. Bridge Fraction and Chain Extension in the Simulated Systems

notation	ϕ_{bridge}	$\langle R_{2L}\rangle^a$	$\langle R_{2B}\rangle^b$	$\langle R\rangle^c$	$\langle R_{2L}\rangle/\langle R\rangle$	$\langle R_{2B}\rangle/\langle R\rangle$
BAB-20	0.50 ± 0.005	9.4	10.4	9.0	1.05	1.16
BAB-30	0.49 ± 0.009	20.8	21.3	17.7	1.18	1.20
BAB-60	0.37 ± 0.011	39.2	39.4	39.6	0.99	0.99

[a] $\langle R_{2L}\rangle = \langle R_{1L}\rangle = \langle R_L\rangle$ the magnitude of vectors $\mathbf{R}_1$ and $\mathbf{R}_2$ for the loops (Figure 1). [b] The magnitude of vector $\mathbf{R}_2$ for the bridges (Figure 1). [c] The magnitude of vector $\mathbf{R}$ for the respective diblock (Figure 1).

The values for ϕ_{bridge} estimated from the computer simulations can be compared to the equilibrium values calculated by theory. Matsen and Shick[6] used a mean-field lattice formalism and found that the bridge fraction changes from ~0.44 for low χN, ~20, to an almost constant value of 0.37 at high χN, ~300. Matsen[16] used a self-consistent-field theory as well as a numerical simulation of the strong segregation theory equations to obtain very similar values. An even more recent estimation by Jones et al.[7] gives values ranging from 0.65 at low χN, ~20, to 0.55 for high χN, ~104 (the renormalized fractions q' they suggest to use range from 0.48 to 0.38). Limiting expressions were also presented in the limit of very high χN.[15,14,7,17] The computer-simulation estimates presented here fall in the same regime of ϕ_{bridge} values, which, however, show a dependence on N and not on the product χN (the calculations for the different systems were performed at the same $T/N = 0.05$, i.e., at the same thermodynamic state). Estimates at different T/N (e.g., at $T/N = 0.10$) did not show a significant effect on ϕ_{bridge} (the obtained values were within the errors of Table 4) as long as the system was well in the ordered state. Therefore, it appears that the bridge fraction depends explicitly on N and not on χN, at least in the present range of molecular weights and χN's.

Because the chains having loop or bridge conformation have been identified, one can examine their individual conformational characteristics (and later their dynamics) in the ordered state and compare them with the respective diblocks. Table 4 shows the estimated average magnitude of the vector $\mathbf{R}_2$ connecting the endpoint to the midpoint of the midblock (Figure 1) for the chains forming loops, $\langle R_{2L}\rangle$, and for those forming bridges, $\langle R_{2B}\rangle$, relative to the magnitude of the end-to-end vector of the block of the respective diblock, $\langle R\rangle$. The midblocks of the triblock chains appear to be more extended than the tails of the diblocks, with this difference apparently disappearing at higher N's. Moreover, the chains having bridge conformation are somewhat more extended than the loops, in agreement with

earlier experimental data.[52]

Dynamic Properties. The aim of the simulation of the dynamics is to be able to discuss the findings in relation to the experimental data presented in section III in order to understand the contribution of loops and bridges on the dielectric relaxation discussed above. For this, the orientational dynamics of the vector $\Delta\mathbf{R} = \mathbf{R}_1 + \mathbf{R}_2$ is investigated individually for chains with loop and bridge conformation of the midblock of the triblock and compared with the respective correlation functions for the end-to-end vector $\mathbf{R}$ of the active block of the diblock.

The dielectric relaxation is related (see Appendix A) to the correlation functions

$$C_{\langle\Delta R\rangle,\mathrm{all}}(t) = \left\langle \frac{1}{n_c^2}\sum_{i=1}^{n_c}\sum_{l=1}^{n_c}\Delta\mathbf{R}_i(t)\cdot\Delta\mathbf{R}_l(0)\right\rangle \tag{9a}$$

and

$$C_{\langle R\rangle,\mathrm{all}}(t) = \left\langle \frac{1}{n_c^2}\sum_{i=1}^{n_c}\sum_{l=1}^{n_c}\mathbf{R}_i(t)\cdot\mathbf{R}_l(0)\right\rangle \tag{9b}$$

for the triblock and the diblock, respectively, where n_c is the total number of chains, $\cdot$ signifies the dot product, and the average $\langle\cdots\rangle$ is taken over the various configurations of the system. The total dielectric strengths are given by

$$\Delta\epsilon_{\mathrm{total,triblock}} \propto C_{\langle\Delta R\rangle,\mathrm{all}}(0) - C_{\langle\Delta R\rangle,\mathrm{all}}(\infty) = \langle(\Delta\mathbf{R})^2\rangle_{\mathrm{all}} \tag{10a}$$

$$\Delta\epsilon_{\mathrm{total,diblock}} \propto C_{\langle R\rangle,\mathrm{all}}(0) - C_{\langle R\rangle,\mathrm{all}}(\infty) = \langle(\mathbf{R})^2\rangle_{\mathrm{all}} \tag{10b}$$

where,

$$\langle(\Delta\mathbf{R})^2\rangle_{\mathrm{all}} = \left\langle \frac{1}{n_c^2}\Big(\sum_{i=1}^{n_c}\Delta\mathbf{R}_i\Big)^2\right\rangle = C_{\langle\Delta R\rangle,\mathrm{all}}(0) \tag{11a}$$

and

$$\langle(\mathbf{R})^2\rangle_{\mathrm{all}} = \left\langle \frac{1}{n_c^2}\Big(\sum_{i=1}^{n_c}\mathbf{R}_i\Big)^2\right\rangle = C_{\langle R\rangle,\mathrm{all}}(0) \tag{11b}$$

Note that $C_{\langle\Delta R\rangle,\mathrm{all}}(\infty) = 0$ and $C_{\langle R\rangle,\mathrm{all}}(\infty) = 0$, because the orientations of $\Delta\mathbf{R}$ and $\mathbf{R}$ are completely uncorrelated for *infinite* times.

Performing the averaging over all of the chains in the system results in very poor statistics. Thus, the correlation functions of the vectors $\Delta\mathbf{R}$ and $\mathbf{R}$ are calculated by taking into account the near neighbors, essentially accounting for the possible existence of correlations on the chain motion only over the near neighbors; this is also consistent with the way the experimental dielectric strength is obtained (it practically originates from the average polarization within a finite volume around each chain). Therefore, the calculated quantities are the following:

$$C_{\langle\Delta R\rangle,\mathrm{neigh}}(t) = \left\langle \frac{1}{n_c}\sum_{i=1}^{n_c}\left[\left(\frac{1}{z}\sum_{j=1}^{z}\Delta\mathbf{R}_{ij}(t)\right)\cdot\left(\frac{1}{z}\sum_{k=1}^{z}\Delta\mathbf{R}_{ik}(0)\right)\right]\right\rangle \tag{12a}$$

$$C_{\langle R\rangle,\mathrm{neigh}}(t) = \left\langle \frac{1}{n_c}\sum_{i=1}^{n_c}\left[\left(\frac{1}{z}\sum_{j=1}^{z}\mathbf{R}_{ij}(t)\right)\cdot\left(\frac{1}{z}\sum_{k=1}^{z}\mathbf{R}_{ik}(0)\right)\right]\right\rangle \tag{12b}$$

$$\langle(\Delta\mathbf{R})^2\rangle = \left\langle \frac{1}{n_c}\sum_{i=1}^{n_c}\left(\frac{1}{z}\sum_{j=1}^{z}\Delta\mathbf{R}_{ij}\right)^2\right\rangle \tag{13a}$$

$$\langle(\mathbf{R})^2\rangle = \left\langle \frac{1}{n_c}\sum_{i=1}^{n_c}\left(\frac{1}{z}\sum_{j=1}^{z}\mathbf{R}_{ij}\right)^2\right\rangle \tag{13b}$$

with $\langle(\Delta\mathbf{R})^2\rangle = C_{\langle\Delta R\rangle\mathrm{neigh}}(0)$ and $\langle(\mathbf{R})^2\rangle = C_{\langle R\rangle,\mathrm{neigh}}(0)$, where z is the number of near neighbors of chain i. Test runs showed that the findings discussed below are not affected in any appreciable way when eqs 12 and 13 are used instead of eqs 9−11; i.e., the assumption that the cross-correlation survives only for neighboring chains does not significantly modify the observed behavior.

Alternatively, the correlation functions can be calculated only over the self-terms, i.e., without taking into account any cross-correlations as

$$C_{\langle\Delta R\rangle}(t) = \left\langle \frac{1}{n_c}\sum_{i=1}^{n_c}\Delta\mathbf{R}_i(t)\cdot\Delta\mathbf{R}_i(0)\right\rangle \tag{14a}$$

$$C_{\langle R\rangle}(t) = \left\langle \frac{1}{n_c}\sum_{i=1}^{n_c}\mathbf{R}_i(t)\cdot\mathbf{R}_i(0)\right\rangle \tag{14b}$$

This calculation is performed only for comparison.

When multiple relaxation processes are involved, the respective $\Delta\epsilon$ should be calculated as the differences $C(t_{\mathrm{start}}) - C(t_{\mathrm{end}})$, with t_{start} and t_{end} signifying the range of the respective relaxation; this leads to the following expressions for the dielectric strengths of the chain relaxation

$$\Delta\epsilon_{\mathrm{triblock}} \propto \langle(\Delta\mathbf{R})^2\rangle^* = \langle(\Delta\mathbf{R})^2\rangle \times \text{(amplitude of the chain process of } C_{\langle\Delta R\rangle,\mathrm{all}}(t)) \tag{15a}$$

$$\Delta\epsilon_{\mathrm{diblock}} \propto \langle(\mathbf{R})^2\rangle^* = \langle(\mathbf{R})^2\rangle \times \text{(amplitude of the chain process of } C_{\langle R\rangle,\mathrm{all}}(t)) \tag{15b}$$

Figure 9 shows the comparison between the normalized $C_{\langle R\rangle,\mathrm{neigh}}(t)/C_{\langle R\rangle,\mathrm{neigh}}(0)$ and $C_{\langle R\rangle}(t)/C_{\langle R\rangle}(0)$ for the three diblock copolymers AB-10 (a), -15 (b), and -30 (c). The two types of correlation functions exhibit the same relaxation times, whereas the reduced statistics result in higher noise for the $C_{\langle R\rangle,\mathrm{neigh}}(t)$ correlation function. The correlation functions do not decay to zero because of the residual memory of $\mathbf{R}$ of the blocks tethered at the lamellar interfaces (this memory relaxes slowly through the interfacial relaxation process in the ordered state;[24,34] the relative amplitude of the latter is higher in the $C_{\langle R\rangle,\mathrm{neigh}}(t)$ correlation function). It is important to note that the dynamics of the fast process does not depend on whether $C_{\langle R\rangle,\mathrm{neigh}}(t)$ or $C_{\langle R\rangle}(t)$ is used. The same is true (with larger uncertainty due to the even poorer statistics) if the correlation function over all chains is calculated. The above hold for the behavior of the correlation functions for the triblock copolymers as well.

Figure 10 shows the normalized correlation functions $C_{\langle\Delta R\rangle,\mathrm{neigh}}(t)/C_{\langle\Delta R\rangle,\mathrm{neigh}}(0)$ for the vector $\Delta\mathbf{R}$ calculated individually for loops and bridges for the triblocks BAB-

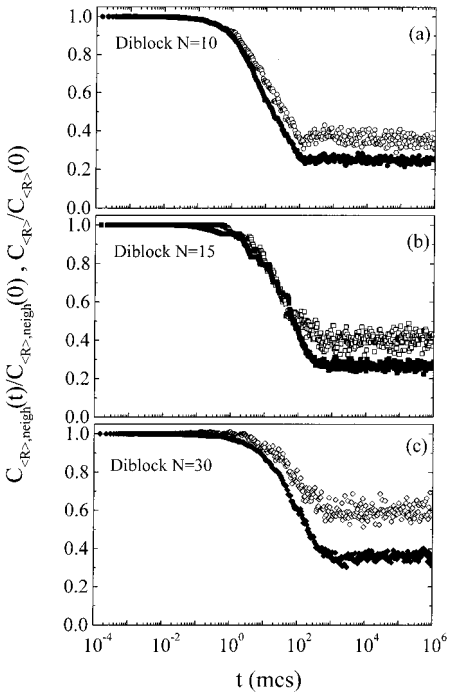

Figure 9. Comparison between the normalized correlation functions $C_{\langle R\rangle,neigh}(t)/C_{\langle R\rangle,neigh}(0)$ (○, □, ◇) and $C_{\langle R\rangle}(t)/C_{\langle R\rangle}(0)$ (●, ■, ◆) for the three diblock copolymers: (a) AB-10 (○, ●), (b) AB-15 (□, ■), and (c) AB-30 (◇, ◆) calculated according to eqs 12b and 14b. Time is expressed in Monte Carlo steps per monomer (mcs).

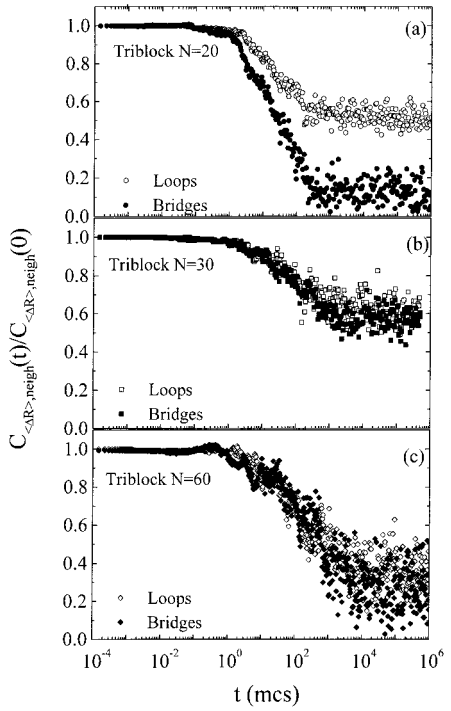

Figure 10. Normalized correlation functions $C_{\langle\Delta R\rangle,neigh}(t)/C_{\langle\Delta R\rangle,neigh}(0)$ for the vector $\Delta\mathbf{R}$ calculated individually for loops (○, □, ◇) and bridges (●, ●, ◆) according to eq 12a for the triblock copolymers: (a) BAB-20 (○, ●), (b) BAB-30 (□, ■), and (c) BAB-60 (◇, ◆). Time is expressed in Monte Carlo steps per monomer (mcs).

20 (a), -30 (b), and -60 (c) for which the bridge and loop chains have been identified. It is evident that the dynamics of the fast process is practically the same for loops and bridges for BAB-30 and -60, whereas for BAB-20, the bridge dynamics appear somewhat faster. Similarly to the case for the diblocks, the correlation functions do not decay to zero due to the slow interface-related process discussed above; the amplitude of this process for diblocks is known to depend on the coherence of the ordered lamellae structure,[24,34] which is not possible to control. Thus, for comparison of the "strength" of the relaxation of $\Delta\mathbf{R}$ (triblocks) to that of $\mathbf{R}$ (diblocks) as well as with the experimentally determined dielectric strengths,[53] one utilizes eq 15a,b, with the amplitudes therein being evaluated using Figures 9 and 10 (the amplitudes are evaluated for the fast mechanism related to the orientational relaxation of $\Delta\mathbf{R}$ or $\mathbf{R}$). The results are summarized in Table 5, where the values of $\langle(\Delta\mathbf{R})^2\rangle^*$ are shown individually for loops and bridges together with the value of $\langle(\mathbf{R})^2\rangle^*$.

Table 5. Comparison of $\langle(\Delta\mathbf{R})^2\rangle^*$, $\langle(\mathbf{R})^2\rangle^*$, and κ Values for the Simulated Systems

notation	$\langle(\Delta\mathbf{R})^2\rangle^*_L$	$\langle(\Delta\mathbf{R})^2\rangle^*_B$	$\langle(\mathbf{R})^2\rangle^*$	$(1-\phi_{bridge})\langle(\Delta\mathbf{R})^2\rangle^*_L$	$\phi_{bridge}\langle(\Delta\mathbf{R})^2\rangle^*_B$	κ
BAB-20	8.0	5.9	1.5	4.0	2.9	2.4 ± 0.14
BAB-30	14.7	8.1	2.0	7.6	3.9	2.9 ± 0.37
BAB-60	26.4	22.9	4.9	16.7	8.4	2.5 ± 0.34

In Table 5, κ defined as

$$\kappa = \frac{0.5[(1-\phi_{bridge})\langle(\Delta\mathbf{R})^2\rangle^*_L + \phi_{bridge}\langle(\Delta\mathbf{R})^2\rangle^*_B]}{\langle\mathbf{R}_2^2\rangle^*} \quad (16)$$

corresponds to the experimentally determined ratio $\Delta\epsilon_{n,triblock}/\Delta\epsilon_{n,diblock}$, provided that the loop and bridge dynamics cannot be separated.[54] In eq 16, $\langle(\Delta\mathbf{R})^2\rangle^*_L$ is the value of $\langle(\Delta\mathbf{R})^2\rangle^*$ for chains forming loops, and $\langle(\Delta\mathbf{R})^2\rangle^*_B$ is that for chains forming bridges whereas the ϕ_{bridge} values from Table 4 are used. The much larger contribution of the chains forming loops to the intensity relative to that of bridges is evident in Table 5 for the low-molecular-weight triblocks ($N = 20$ and 30). Actually, since the fraction of bridges was estimated (Table 4) to be about 50% for these, the total contribution of loops to κ is about twice that of bridges for these low-molecular-weight systems (Table 5). For $N = 60$, the difference in the two quantities $\langle(\Delta\mathbf{R})^2\rangle^*_L$ and $\langle(\Delta\mathbf{R})^2\rangle^*_B$ becomes less; however, even in this case with the bridge fraction $\phi_{bridge} \cong 37\%$ (Table 4), the total contribution of loops to κ is again twice that of the bridges (Table 5). Moreover, for all N's, the ratio κ is larger than unity and around 2.5 is in close agreement with the experimental observation for the annealed samples of $\Delta\epsilon_{n,triblock}/\Delta\epsilon_{n,diblock} \cong 2$.

Figure 11 shows a comparison between the normalized correlation functions $C_{\langle\Delta R\rangle,neigh}(t)/C_{\langle\Delta R\rangle,neigh}(0)$ for the loops of the triblocks and $C_{\langle R\rangle,neigh}(t)/C_{\langle R\rangle,neigh}(0)$ for the diblocks together with the respective relaxation spectra $\tilde{F}(\ln\tau)$, obtained by the CONTIN[29,30] inversion of the correlation functions. In all cases, the distributions of relaxation times for the loops are much broader than for those for the respective diblocks while the relaxation times are not very different. Actually, the most probable relaxation time (the peak of $\tilde{F}(\ln\tau)$) of the $C_{\langle R\rangle,neigh}(t)$ for the diblocks is somewhat faster than that for the $C_{\langle\Delta R\rangle,neigh}(t)$ for the loops of the triblocks, with this difference being larger for the highest molecular weight (a factor of ~5). The broader distribution leads to the expectation of a broader dielectric loss for the triblock, in agreement with the experiment in the annealed systems, whereas the dynamics does not appear faster, *in disagreement* with the experiment.

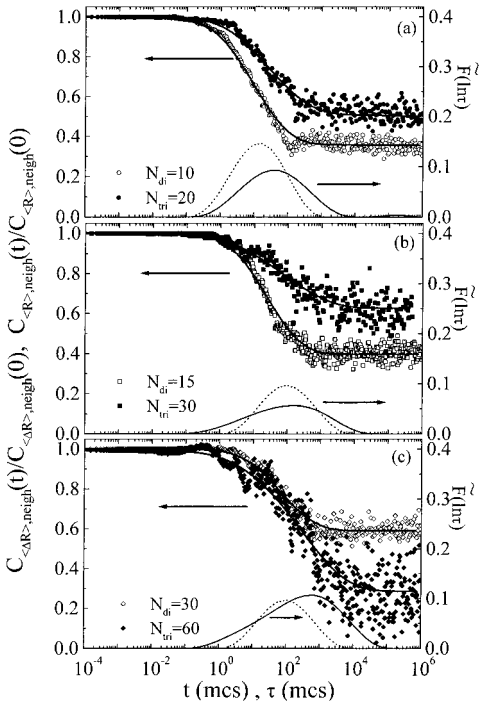

Figure 11. Comparison between the normalized correlation functions $C_{\langle R\rangle,neigh}(t)/C_{\langle R\rangle,neigh}(0)$ for the diblocks (○, □, ◇) and $C_{\langle \Delta R\rangle,neigh}(t)/C_{\langle \Delta R\rangle,neigh}(0)$ for the loop conformation in triblocks (●, ■, ◆) for (a) AB-10 (○) and BAB-20 (●), (b) AB-15 (□) and BAB-30 (■), and (c) AB-30 (◇) and BAB-60 (◆), together with the distributions of relaxation times $\tilde{F}(\ln\tau)$ (solid line for the triblocks and dotted line for the diblocks; right axis). Time is expressed in Monte Carlo steps per monomer (mcs).

Possible origins of disagreement may be the different degree of entanglement between the real polyisoprene midblock chains and the simulated systems[55] and, even more importantly, the fact that in the experiment the ends of the midblock chains are practically frozen at the interfacial regions with the glassy polystyrene lamellae (the temperature range of the experiments is below the polystyrene glass-transition temperature), whereas in the simulations, both components possess the same mobilities. This means that these simulations are concerned with the investigation of the true (but hard to realize) equilibrium features of the midblock loop and bridge dynamics. A series of simulations with varying friction coefficient ratios between A and B can be useful for a closer correlation with the experimental data; however, because of the computation time requirements (it will increase proportionally to the ratio of friction coefficients), this is left for a future work.

V. Concluding Remarks

Dielectric relaxation spectroscopy and Monte Carlo computer simulations have been utilized to probe the bridges-to-loops ratio in ordered symmetric triblock copolymers. In an extension/completion of an earlier work by Watanabe,[19] the effects of the sample history on the dielectric relaxation behavior of triblock copolymers with symmetrically inverted dipoles along the chain backbone of the middle block have been investigated. For specimens with quenched chain configurations when the number fraction of knotted loops or bridges is small, the dielectric method is capable within certain assumptions (either that of the loops dominating the low-frequency response or that of the bridges having a negligible amplitude) to identify the unknotted bridge fraction utilizing the fact that the slow dynamics in the triblock are essentially due to the unknotted loops; at this moment, it seems that this method is the best and only method for a simple determination of ϕ_{bridge}. However, it is found that, with annealing, a process with dynamics intermediate between the segmental mode and the block relaxation of the respective diblock develops having a much higher intensity. This is probably due to the annealing affecting the conformation of the midblock chains and especially the fraction of interdigitated (knotted) loops and bridges and rendering almost impossible the estimation of the bridge fraction.

Monte Carlo computer simulations using the Cooperative Motion Algorithm were used to identify the bridge fraction in the static mode as well as the characteristics of the orientational motion of midblock chains having either loop or bridge conformation and compare their contributions to the total dielectric response relative to that of the respective diblocks. The equilibrium bridge fraction is estimated as 0.50−0.37, in the same range with theoretical predictions; however, it decreases with N at constant $T/N = 0.05$, whereas theory predicts that it is only a function of χN. It is found that at true equilibrium the contribution of the intensity of loops is almost twice that of bridges, with both, however, having similar relaxation rates. The total intensity is much larger than that for the respective diblocks, in agreement with the experiment for the annealed triblocks. The dynamics is found to be very similar to that for the normal mode in the diblocks, which does not agree with the observed behavior for the annealed systems. This should be due to the different dynamic state of the end-block domains between the simulated (equal mobilities) and the actual experimental system (glassy polystyrene), which provides an extra thermodynamic constraint for the chain motion of the polyisoprene midblock.

At temperatures lower than the glass transition of the polystyrene domains, where the block junction is essentially frozen and the system is in the quenched (partial equilibrium) state, the ϕ_{bridge} value determined experimentally is not the true equilibrium value but gives a real bridge fraction in the quenched systems. The simulations suggest that at higher temperatures (higher than T_g^{PS}) the bridge fraction in the system would be closer to the true equilibrium value but its dielectric evaluation may become difficult because of the reduction of the dynamic differences between the loop and bridge conformations due to the enhanced junction mobility.

Acknowledgment. S.H.A. acknowledges that part of this research was sponsored by NATO's Scientific Affairs Division in the framework of the Science for Stability Programme and by the Greek General Secretariat of Research and Technology. T.P. acknowledges partial support of the Alexander von Humboldt Foundation under Grant Number FOKOOP USS1685. We thank Professor J. T. Koberstein for valuable discussions on the subject, Professor F. Kremer for his collaboration with the initial dielectric measurements, and Ms. K. Chrissopoulou for her assistance.

Appendix A: Framework of Dielectric Spectroscopy Relevant to the Present Work

Dielectric relaxation spectroscopy was used to investigate the collective chain dynamics of the PI blocks of

the di- and triblocks in the ordered state. The complex dielectric permittivity (section II) is given by the one-sided Fourier transform of the time derivative of the autocorrelation function of the *z*-component of the polarization, $C(t) = \langle P_z(t)P_z(0)\rangle$. The evaluation of this $C(t)$ for the present di- and triblock systems and its relationship to the dielectric loss $\epsilon''(\omega)$ is summarized below.

1. Expression of $C(t)$ for PI. The PI chain possesses segmental dipole components both parallel and perpendicular to the chain backbone. For the PI block of the diblock examined in this study, the parallel dipoles are aligned in the same direction along the block backbone. Thus, for this block (indexed with α), the sum of these dipoles is proportional to its end-to-end vector $\mathbf{R}_\alpha$ (cf. Figure 1). On the other hand, for the PI block of the triblock, the parallel dipoles are once inverted at its midpoint. For this case, the sum of these dipoles is proportional to the vector $\Delta\mathbf{R}_\alpha = \mathbf{R}_{1\alpha} + \mathbf{R}_{2\alpha}$, where $\mathbf{R}_{1\alpha}$ and $\mathbf{R}_{2\alpha}$ are the two vectors connecting the end to the midpoint of the PI block; see Figure 1. Therefore, the polarization of the αth copolymer chain at $T < T_g^{PS}$ (where the PS block motion is frozen) is given by $\mathbf{p}_\alpha(t) = \mu\mathbf{R}_\alpha(t) + \sum_\beta \mu'_{\alpha,\beta}(t)$ for the diblock and $\mathbf{p}_\alpha(t) = \mu\Delta\mathbf{R}_\alpha(t) + \sum_\beta \mu'_{\alpha,\beta}(t)$ for the triblock. Here, μ is the magnitude of the parallel dipole reduced to unit end-to-end distance, and $\mu'_{\alpha,\beta}$ is the perpendicular dipole of a βth PI segment of this chain.

In the di- and triblock copolymer systems, the fluctuation of $\mu'_{\alpha,\beta}(t)$ due to the local (segmental) motion at $t > 0$ can be assumed to be uncorrelated with $\mathbf{R}_\alpha(0)$ or $\Delta\mathbf{R}_\alpha(0)$, i.e., the quantities specifying the global chain configuration in the initial state ($t = 0$).[28,29] Similarly, the fluctuation of $\mathbf{R}_\alpha(t)$ or $\Delta\mathbf{R}_\alpha(t)$ due to the global chain motion can be assumed to be uncorrelated with the initial values $\mu'_{\alpha,\beta}(0)$. Under these assumptions, we can utilize the above expression of $\mathbf{p}_\alpha$ to write $\Delta C(t) = C(t) - C(\infty)$ in the form

$$\Delta C(t) = \Delta C^{\parallel}(t) + \Delta C^{\perp}(t) \tag{A1}$$

with

$$\Delta C^{\parallel}(t) = \mu^2 \sum_\alpha \sum_{\alpha'} [\langle R_{z,\alpha}(t) R_{z,\alpha'}(0)\rangle - \langle R_{z,\alpha}(\infty) R_{z,\alpha'}(0)\rangle] \quad \text{[diblock]} \tag{A2}$$

$$\Delta C^{\parallel}(t) = \mu^2 \sum_\alpha \sum_{\alpha'} [\langle \Delta R_{z,\alpha}(t) \Delta R_{z,\alpha'}(0)\rangle - \langle \Delta R_{z,\alpha}(\infty) \Delta R_{z,\alpha'}(0)\rangle] \quad \text{[triblock]} \tag{A3}$$

$$\Delta C^{\perp}(t) = \sum_\alpha \sum_{\alpha'} \sum_\beta \sum_{\beta'} [\langle [\mu'_{\alpha,\beta}(t)]_z [\mu'_{\alpha',\beta'}(0)]_z\rangle - \langle [\mu'_{\alpha,\beta}(\infty)]_z [\mu'_{\alpha',\beta'}(0)]_z\rangle] \tag{A4}$$

$R_{z,\alpha}(t)$, $\Delta R_{z,\alpha}(t)$, and $[\mu'_{\alpha,\beta}(t)]_z$ are, respectively, the components of $\mathbf{R}_\alpha(t)$, $\Delta\mathbf{R}_\alpha(t)$, and $\mu'_{\alpha,\beta}(t)$ in the direction of $\mathbf{E}$ (*z*-direction). The relaxation of $\Delta C^{\perp}(t)$ is induced by the fast segmental motion, whereas that of $\Delta C^{\parallel}(t)$ results from the much slower global chain motion (normal mode relaxation). Thus, $\Delta C(t)$ splits into fast and slow relaxation functions ($\Delta C^{\perp}$ and $\Delta C^{\parallel}$) that are experimentally observed at low and high temperatures, respectively.

2. Interchain Correlation in $C^{\parallel}(t)$. The $\Delta C^{\parallel}(t)$ for the global mode includes (eqs A2 and A3) both autocorrelation terms (with $\alpha' = \alpha$) and the cross-correlation (interchain correlation) terms (with $\alpha' \neq \alpha$). The net contribution of the latter terms to $\Delta C^{\parallel}(t)$ changes with the chain conformation. The di- and triblock copolymers examined dielectrically have an (almost) identical lamellar structure parallel to the electrodes. However, the conformation of the PI blocks is different, as schematically shown in Figure 2. In the diblock, all PI blocks attain the tail conformation, whereas, in contrast, the PI blocks in the triblock lamella take various conformations, i.e., the unknotted (dangling) loop, the unknotted bridge, and the loop/bridge mutually knotted in various ways.

For the tails, the cross-correlation contribution to $\Delta C^{\parallel}$ was discussed by Yao et al.[21a] They examined the dielectric behavior of blends of PS−PI and PS−polybutadiene (PB) diblocks of almost identical molecular weights and composition (PS:diene ≅ 50:50). These copolymers were uniformly mixed to coform PS/diene alternating lamellae. Because the PB block does not possess a parallel dipole component, the slow dielectric relaxation of this mixed lamella was exclusively attributed to the global motion of the PI blocks. Their data indicated that the dielectric relaxation intensity was proportional to the PI block concentration c_{PI} whereas the dielectric mode distribution was insensitive to c_{PI}. The pairwise cross-correlation would have resulted in a scaling of the intensity as c_{PI}^2 as well as in changes of the mode distribution with c_{PI} because the correlation between the dielectrically active PI chains is reduced on dilution by the inert PB blocks, i.e., on decreasing c_{PI}. Thus, those data indicate that the cross-correlation contributes negligibly to $\Delta C^{\parallel}(t)$ of the PS−PI diblock copolymer lamella.

This lack of the cross-correlation contribution indicates that a cancellation occurs for the cross-correlation terms in eq A2 for the PI tails in the diblock lamella.[35] Equal numbers of PI tails are tethered on the top and bottom surfaces of the lamella shown in Figure 2a. Thus, for a given (αth) PI tail having $\mathbf{R}_\alpha(t)$, the other (α′th) tails have their end-to-end vectors $\mathbf{R}_{\alpha'}(0)$ and $-\mathbf{R}_{\alpha'}(0)$ with the same probability and the sum $\sum_\alpha \sum_{\alpha'\neq\alpha} [\langle R_{z,\alpha}(t) R_{z,\alpha'}(0)\rangle - \langle R_{z,\alpha}(\infty) R_{z,\alpha'}(0)\rangle]$ vanishes. In other words, the cross-correlation does exist for chain motion but has no total dielectric activity. Note that a similar argument holds for homo-PI chains. Thus, for the diblock lamella parallel to the electrode, eq A2 is simply written in terms of the autocorrelation $\Delta c_t^{\parallel}(t)$ for a representative tail[35] (Figure 2a)

$$\Delta C^{\parallel}_{PS-PI}(t) = 2\nu \Delta c_t^{\parallel}(t) \tag{A5}$$

with

$$\Delta c_t^{\parallel}(t) = \mu^2 [\langle H(t)H(0)\rangle - \langle H(\infty)H(0)\rangle] \quad \text{for a tail} \tag{A6}$$

where 2ν is the number density of the PI tails in the system and $H(t)$ is the free end height of this tail at time t measured from the bottom surface of the lamella shown in Figure 2a ($H = R_z$).

For the unknotted loops and bridges in the triblock lamella (Figure 2b,c), a similar cancellation occurs, and the sum $\sum_\alpha \sum_{\alpha'\neq\alpha} [\langle \Delta R_{z,\alpha}(t) \Delta R_{z,\alpha'}(0)\rangle - \langle \Delta R_{z,\alpha}(\infty) \Delta R_{z,\alpha'}(0)\rangle]$ in eq A3 vanishes. Thus, for these unknotted chains, $\Delta C^{\parallel}(t)$ is written as

$$\Delta C^{\parallel}(t) = \sum_{\xi} \nu_\xi \Delta c_\xi^{\parallel}(t), \quad \xi = \text{u.l. (unknotted loops) and u.b. (unknotted bridge)} \tag{A7}$$

where ν_ξ is the number density of the unknotted loops

or bridges in the system and $\Delta c_{\xi}^{\parallel}(t)$ is the autocorrelation for the representative chains shown in Figure 2b,c[35]

$$\Delta c_{\text{u.l.}}^{\parallel}(t) = 4\mu^2[\langle H(t)H(0)\rangle - \langle H(\infty)H(0)\rangle] \quad \text{for an unknotted loop} \quad \text{(A8)}$$

$$\Delta c_{\text{u.b.}}^{\parallel}(t) = 4\mu^2[\langle D(t)D(0)\rangle - \langle D(\infty)D(0)\rangle] \quad \text{for an unknotted bridge} \quad \text{(A9)}$$

Here, $H(t)$ represents the height of the loop midpoint ($\Delta R_z = 2H$ for the loop), and $D(t)$ denotes a displacement of the bridge midpoint from the lamellar midplane ($D = H - L/2$; $\Delta R_z = 2D$ for the bridge).

The situation is different for knotted chains.[35] The above cancellation would occur for chains belonging to different knots but not for chains included in the same knot. For mutually knotted g chains (loops/bridges), the polarization in the z-direction is given by

$$p_{\text{k}}(t) = 2g\overline{A(t)} \qquad \overline{A(t)} = \frac{1}{g}\sum_{\alpha=1}^{g} A_\alpha(t) \qquad \text{(A10)}$$

where $A_\alpha(t) = \Delta R_z/2$ represents a midpoint configuration of the αth chain in the knot and $\overline{A(t)}$ is an average taken for all g chains in the knot; $A_\alpha(t)$ is the midpoint height $H_\alpha(t)$ or the residual height $L - H_\alpha(t)$ if the αth chain forms a loop tethered on the bottom or top surface of the lamella, respectively, whereas $A_\alpha(t)$ is the midpoint displacement $D_\alpha(t)$ if the αth chain forms a bridge (Figure 2). From this $p_k(t)$ defined for the g chains (n bridges, m loops on the bottom lamellar surface, and $g - n - m$ loops on the top surface), an average contribution to $\Delta C^{\parallel}(t)$ from a chain in the knot is given by

$$\Delta c^{\parallel}{}_{\text{k}}(t;g,n,m) = \frac{1}{g}[\langle p_{\text{k}}(t)p_{\text{k}}(0)\rangle - \langle p_{\text{k}}(\infty)p_{\text{k}}(0)\rangle] = 4g\mu^2[\langle \overline{A(t)}\,\overline{A(0)}\rangle - \langle \overline{A(\infty)}\,\overline{A(0)}\rangle] \quad \text{(A11)}$$

For an ensemble of knots each containing g chains, $\Delta C_{\text{k}}^{\parallel}$ is simply written, in terms of this $\Delta c_{\text{k}}^{\parallel}$, as

$$\Delta C_{\text{k}}^{\parallel}(t;g,n,m) = \nu_{\text{k}}(g,n,m)\Delta c_{\text{k}}^{\parallel}(t;g,n,m) \quad \text{(A12)}$$

where $\nu_{\text{k}}(g,n,m)$ is the number density of the chains included in the above types of knots.

It should be noted, here, that $\Delta c_{\text{k}}^{\parallel}$ of a knotted chain (eq A11) is written in a form similar to $\Delta c^{\parallel}$ of a unknotted chain (eqs A8 and A9), except that $\Delta c_{\text{k}}^{\parallel}$ has an extra front factor g not appearing in eqs A8 and A9. This factor reflects an enhancement of polarization due to cross-correlation of the g chains in a knot.[35] From this factor, one might consider that the dielectric intensity of a chain in a knot ($\propto \Delta c_{\text{k}}^{\parallel}(0)$) is infinitely enhanced for $g \to \infty$. However, the fluctuation of the midpoint, $[\langle \overline{A(t)}\,\overline{A(0)}\rangle - \langle \overline{A(\infty)}\,\overline{A(0)}\rangle]$ in eq A11, is suppressed with increasing g, and the intensity saturates for $g \to \infty$, as suggested by Watanabe et al.;[35] more details are explained in Appendix B.

3. ϵ'' for Diblock and Triblock Lamellae. The dielectric relaxation function of the triblock copolymer lamella, which includes the PI blocks having the various conformations, is therefore given by

$$\Delta C_{\text{PS-PI-PS}}^{\parallel}(t) = \nu_{\text{u.l.}}\Delta c_{\text{u.l.}}^{\parallel}(t) + \nu_{\text{u.b.}}\Delta c_{\text{u.b.}}^{\parallel}(t) + \sum_{g\geq 2}\sum_{n\geq 0}\sum_{m\geq 0} \nu_{\text{k}}(g,n,m)\Delta c_{\text{k}}^{\parallel}(t;g,n,m) \quad \text{(A13)}$$

The first and second terms represent the contributions from the unknotted loops and bridges, respectively, and the last term indicates the contribution from all knotted loops/bridges. Here, the total number density of the triblock chains is half of the density of the diblock chains; i.e., $\nu_{\text{u.l.}} + \nu_{\text{u.b.}} + \nu_{\text{k}}^T = \nu$, with $\nu_{\text{k}}^T = \sum_{g\geq 2}\sum_{n\geq 0}\sum_{m\geq 0} \nu_{\text{k}}(g,n,m)$ (total number density of the knotted chains). Thus, if one knows or guesses some details of the relaxation functions of the diblock and triblock chains, $\Delta c_{\xi}^{\parallel}(t)$ with $\xi = t$ (eq A6), u.l. (eq A8), u.b. (eq A9), and k (eq A11), the comparison of the dielectric data of the triblock and diblock lamellae enables one to estimate the unknotted bridge fraction, $\phi_{\text{u bridge}} = \nu_{\text{u.b.}}/\nu$. The details of those relaxation functions in turn reflect characteristic features of the block chain motion.

The block chains are spatially confined in a lamella and are thermodynamically required to preserve their bulk segment density. These two factors, the spatial confinement and the density-preserving requirement, influence the chain motion and, thus, determine the relaxation functions. When one examines these effects, it is informative to first study the dielectric behavior under the absence of these factors; as summarized in Appendix B, a model calculation[35] indicates that the dielectric behavior is exactly the same for tails, unknotted loops, and unknotted bridges, with the latter two having the dipole inversion at the midpoint. The behavior of the knotted loops/bridges cannot be rigorously calculated because a topological constraint due to the knot is not simply represented in terms of the chain conformation. However, in an extreme case of the strongest constraint where the knot behaves as a cross-linking node, the knotted chains can be modeled as a bundle of tails that are connected at their ends. A calculation for this model[35] indicates that the behavior of the bundle is the same as that of the unknotted chains. In the other extreme of the weakest constraint, i.e., when the knot has no effect, the behavior of the unknotted loop/bridge is recovered. Thus, the behavior in these two extremes is identical. This result suggests that the diblock and triblock lamellae exhibit essentially the same dielectric response (and thus the tail, loop, and bridge are not dielectrically distinguished) if the block chains are *not* subjected to the spatial confinement and the density-preserving requirement. For chains that are subjected only to the spatial confinement in a lamella, the model calculation indicates[35] that the dielectric behavior is the same for the unknotted loop and bridge and only a minor difference in the dielectric intensity is noted for the tail. No difference is found for knotted loops and bridges modeled as the bundle, and the dielectric intensity is moderately larger for these knotted chains than for the unknotted chains. More importantly, it was pointed out that the spatial confinement itself moderately accelerates the block chain relaxation, and this effect is just the opposite of the observed one. From these results, it was demonstrated that the block chain dynamics is much more significantly affected by the thermodynamic requirement of preserving constant density.[35]

In previous studies,[19,26] Watanabe and co-workers discussed the similarity/differences in the dynamics of the tail and unknotted loops/bridges under the influence

of this thermodynamic effect. The block chains move in a highly cooperative way so that their motion does not violate the density-preserving requirement, and this cooperativity forces the chains to take even entropically unfavorable distorted configurations before they relax. This entropic barrier results in the retarded and broadened dielectric relaxation of the block chains. A conformational and motional similarity between the tail and the unknotted loop and a difference between the tail and the bridge was considered in order to argue that the dielectric relaxation is similar for the tail and loop (except that the loop is composed of two tails connected at the ends and its dielectric intensity is twice of the intensity of the tail), whereas the relaxation would be faster and the intensity smaller for the bridge.[19,26] This argument leads to a relationship $\Delta c^{\parallel}_{\text{u.l.}}(t) \cong 2\Delta c^{\parallel}_{t}(t) \gg \Delta c^{\parallel}_{\text{u.b.}}(t)$ at long times. *If* the knotted chains do not significantly contribute to $\Delta C^{\parallel}_{\text{PS-PI-PS}}$ of the triblock lamella, i.e., if the population ν^{T}_{k} of those chains is considerably smaller than the populations $\nu_{\text{u.l.}}$ and $\nu_{\text{u.b.}}$ of the unknotted loops and bridges, the above relationship is rewritten as (cf. eqs A5 and A13)

$$\Delta C^{\parallel}_{\text{PS-PI-PS}}(t) \cong 2\nu_{\text{u.l.}}\Delta c^{\parallel}_{t}(t) = (\nu_{\text{u.l.}}/\nu)\Delta C^{\parallel}_{\text{PS-PI}}(t) \quad \text{at long } t \quad \text{(A14)}$$

where the ratio $(\nu_{\text{u.l.}}/\nu)$ is identical to the unknotted loop fraction $\phi_{\text{u.loop}}$ (for the case $\nu^{T}_{\text{k}} \ll \nu$ considered here). For the measured quantity ϵ'', eq A14 can be cast in the form[19,26]

$$\epsilon''_{\text{PS-PI-PS}}(\omega) \cong \phi_{\text{u.loop}}\epsilon''_{\text{PS-PI}}(\omega) \quad \text{at low } \omega \quad \text{(A15)}$$

Thus, if the above argument is valid, the ω dependence (dielectric mode distribution) is the same for $\epsilon''_{\text{PS-PI-PS}}(\omega)$ and $\epsilon''_{\text{PS-PI}}(\omega)$ of the triblock and diblock lamellae at low ω, and the magnitude is smaller for the former by the factor $\phi_{\text{u.loop}}$. Furthermore, if the second part of the argument is valid, and the dielectric intensity $\Delta\epsilon$ is significantly smaller for the bridge than for the loop (both in the unknotted state), eq A15 holds in a considerably wide range of ω, meaning that $\phi_{\text{u.loop}}$ can be evaluated also from a relationship for $\Delta\epsilon$,

$$\Delta\epsilon_{\text{PS-PI-PS}}(\omega) \cong \phi_{\text{u.loop}}\Delta\epsilon_{\text{PS-PI}}(\omega) \quad \text{(A16)}$$

The dynamic behavior of knotted chains is not (explicitly) included in the argument of Watanabe.[19,26] Thus, if ν^{T}_{k} is comparable to (or larger than) $\nu_{\text{u.l.}}$ and $\nu_{\text{u.b.}}$ and the knotted chains significantly contribute to $\Delta C^{\parallel}_{\text{PS-PI-PS}}$ of the triblock lamella, eqs A15 and A16 may fail. Specifically, it is expected that $\Delta\epsilon_{\text{PS-PI-PS}}$ is considerably larger than $\Delta\epsilon_{\text{PS-PI}}$ if the dielectric response of this lamella is dominated by the knotted chains that mutually enhance their polarization (cf. Appendix B). The ω dependence of $\epsilon''_{\text{PS-PI-PS}}(\omega)$ and $\epsilon''_{\text{PS-PI}}(\omega)$ is examined (section III) to test the validity of the argument (for the case of $\nu^{T}_{\text{k}} \ll \nu$) and $\phi_{\text{u.loop}}$ is estimated from eqs A15 and A16 when this validity is confirmed.

Appendix B. Dielectric Behavior of Tail, Loop, Bridge, and Knotted Chains in the Absence of the Density-Preserving Requirement

For the PI block chains having various conformations, the relaxation function $\Delta C^{\parallel}(t)$ reflects fluctuations of the block end points (for the tail) and midpoints (for loop/bridge) that are shown in Figure 2 with the filled circles. Recently, Watanabe et al.[35] calculated $\Delta C^{\parallel}(t)$ of those chains that are placed in a lamella but *not* subjected to the density-preserving requirement. The $\Delta C^{\parallel}(t)$ was examined in two cases: in the first case, the lamella has freely permeable walls (i.e., the chains are tethered at certain points in free space), whereas in the second case, the lamellar walls are impermeable for the chains, and thus, the effect of spatial confinement emerges. For both cases, the lowest-order motional mode (having the largest wavelength) was considered (if necessary, one can incorporate higher-order motional modes in the calculation, but the analysis for the lowest-order mode is sufficient for demonstration of the effect of spatial confinement). The results obtained[35] are summarized below.

1. Behavior in Free Space. For the tail chain tethered on a permeable lamellar wall at $z = 0$ (Figure 2a), the distribution of the free end position H is described by

$$W_t(H) = \left(\frac{2\pi R_0^2}{3}\right)^{-1/2} \exp\left[-\frac{3H^2}{2R_0^2}\right] \quad (-\infty < H < \infty) \quad \text{(B1)}$$

Here, R_0 is the unperturbed end-to-end distance of the tail ($R_0 = N^{1/2}b$, with N as the number of segments in the tail and b as the segment step length). For the unknotted loop or bridge, i.e., the head-to-head dimer of the tail (Figure 2b,c), the distribution function for the midpoint location is written in terms of this W_t,

$$W_{\text{u.l.}}(H) = C_{\text{u.l.}}[W_t(H)]^2 \quad \text{(unknotted loop)} \quad \text{(B2)}$$

$$W_{\text{u.b.}}(H) = C_{\text{u.b.}}W_t(H)W_t(L - H) \quad \text{(unknotted bridge)} \quad \text{(B3)}$$

Here, L is the lamellar thickness (cf. Figure 2), and $C_{\text{u.l.}}$ and $C_{\text{u.b.}}$ are respective normalization constants. The elastic force acting on the end point/midpoint is calculated as

$$F = \frac{\partial}{\partial H}[k_{\text{B}}T \ln W] \quad \text{(B4)}$$

The balance of this F, a frictional force ($-\zeta\, dH/dt$ for tail and $-2\zeta\, dH/dt$ for loop/bridge, with $\zeta = N\zeta_0$ the friction coefficient of the tail and ζ_0 that of a segment), and the Brownian force F_{B} results in the equation of motion.

For the knotted chains (Figure 2d–f), a topological constraint due to the knot would affect the chain motion. This effect is not simply represented in terms of the chain configuration, and the equation of motion cannot be rigorously formulated. However, in the extreme case where the knot gives the strongest constraint and works as a cross-linking node, the knotted chains can be modeled as a bundle of tails connected at their ends. For the simplest bundle that contain two g tails, each composed of the same number (N) of segments, the distribution function for the node position H is again written in terms of W_t (eq B1)

$$W_{\text{k}}(H) = C_{\text{k}}[W_t(H)]^q[W_t(L - H)]^{2g-q} \quad \text{(B5)}$$

where q is the number of tails tethered on the bottom surface of the lamella (e.g., $q = 2$, 3, and 2 for parts d,

e, and f of Figure 2, all having $g = 2$) and C_k is a normalization constant. A balance of the elastic force calculated from this W_k (eq B4), a frictional force $-2g\zeta$ dH/dt, and F_B gives the equation of motion for the node.

The above equations of motion were solved[35] to obtain $H(t)$ for the respective cases. Utilizing this $H(t)$ or $D(t) = H(t) - L/2$ in eqs A5−A11, $\Delta C^{\parallel}(t)$ was obtained for systems containing 2ν tails per unit volume, or ν unknotted loops/bridges, or ν/g bundles each containing g chains (a model for the ν knotted loops/bridges). The results are the same for all systems including the system of the bundles having any g and q values,[35]

$$\Delta C^{\parallel}(t) = \frac{2}{3}\nu\mu^2 R_0^2 \exp[-t/\tau_f] \qquad \tau_f = \frac{\zeta R_0^2}{3k_B T} \propto N^2 \quad \text{(B6)}$$

The coincidence of $\Delta C^{\parallel}(t)$ for those chains can be also found when the higher-order motional modes are incorporated in the Rouse calculation.[26] The bundle is the model for the knotted chains subjected to the strongest constraint due to the knot. For the case of the weakest constraint (no effect of knot), the same $\Delta C^{\parallel}(t)$ is obtained. Thus, the dielectric behavior should not be affected significantly by the knots and eq B6 should give $\Delta C^{\parallel}(t)$ for any system of chains having various conformations (in free space).

The above results are informative in the following ways: (i) The coincidence of $\Delta C^{\parallel}(t)$ for all systems means that the loops and bridges cannot be dielectrically distinguished if there is no spatial confinement and no density-preserving requirement. (ii) For the bundle, the enhancement of the cross-correlation of the polarization of the chains in the same knot, reflected in the factor g in eq A11, is exactly canceled by a suppression of the fluctuation of the node (as noted from eq B5, the node position distribution becomes narrower, and thus, the node is more strongly bound at its average position for larger g[35]).

2. Behavior in the Lamellae. For the tail that is tethered on the bottom surface of the lamella and just spatially confined in this lamella (i.e., not required to preserve the uniform segment density), the distribution of the free end position H is described by[57]

$$W_t(H) = C_t \sum_{\gamma=-\infty}^{\infty} (H - 2\gamma L) \exp\left[-\frac{3(H - 2\gamma L)^2}{2R_0^2}\right] \qquad (0 \le H \le L) \quad \text{(B7)}$$

where L is the lamellar thickness and C_t a normalization constant. The H dependence of W_t depends on the ratio R_0/L. For example, for $R_0/L \ll 1$, W_t is reduced to the distribution function in a half space[58] ($H \ge 0$), $W_t \propto H \exp[-3H^2/(2R_0^2)]$. For the actual PS−PI and PS−PI−PS lamellae examined in this study, L (=9.5 nm) is close to R_0 (=8.7 nm).[19] The W_t for the case of $L = R_0$ is satisfactorily approximated by a simple parabolic distribution function[35]

$$W_p(H) = \frac{6}{L^3} H(L - H) \quad (0 \le H \le L) \qquad \text{(B8)}$$

Considering these points, this W_p was used[35] to calculated $\Delta C^{\parallel}(t)$ for the systems of tails, unknotted loops/bridges, and bundles (the model for knotted loops/bridges). The calculation procedure was the same as the procedure giving eq B6, except that W_p was used instead of W_t given in eq B1. For all of these chains, the results (for $L = R_0$) are summarized as[35]

Table 6. Dielectric Parameters of Model Chains[35]

	$\nu^{-1}\mu^{-2}R_0^{-2}\Delta C^{\parallel}(0)^a$	Q^b
In Free Space		
any chain	2/3	1
In Lamella with $L = R_0$		
tail	1/10	0.863
loop/bridge	1/7	0.881
bundle ($g = 2$)	2/11	0.907
bundle ($g = 4$)	4/19	0.936
bundle ($g = 8$)	8/35	0.961
bundle ($g = \infty$)	1/4	1

[a] $\Delta\epsilon \propto \Delta C^{\parallel}(0)$. [b] $Q = \nu\mu^2 L^2 I_1/\Delta C^{\parallel}(0)$.

$$\Delta C^{\parallel}(t) = \nu\mu^2 L^2 \sum_{j=0}^{\infty} I_j \exp[-(2j+1)t/\tau_l] \qquad \tau_l = \frac{\zeta L^2}{8k_B T} \propto N^2 \quad \text{(B9)}$$

where I_j is a reduced intensity of the jth relaxation mode and τ_l is the longest relaxation time. Table 6 summarizes the initial values $\Delta C^{\parallel}(0) = \nu\mu^2 L^2 \sum_{j=0}^{\infty} I_j \propto \Delta\epsilon$ and a measure for a degree of polydispersity in the relaxation modes, $Q = \nu\mu^2 L^2 I_1/\Delta C^{\parallel}(0)$. Note that the $\Delta C^{\parallel}(0)$ values were rigorously calculated from W_p but the Q values were obtained from an approximate perturbation calculation;[35] the accuracy of the Q values was estimated to be better than 6%. For comparison, the $\Delta C^{\parallel}(0)$ and Q values for the chains in the free space (eq B6) are also shown in Table 6.

By comparing eqs B9 and B6, it is noted that the relaxation of the chains is moderately faster in the lamellae than in the free space, $\tau_l = (^3/_8)\tau_f$. It is also noted that the relaxation behavior in the lamellae is identical for the loops and bridges (in either unknotted or knotted states), meaning that these two conformations cannot be dielectrically distinguished. These results, obtained for chains that *are not subjected to the density-preserving requirement*, are qualitatively different from the experimental observation. This, in turn, means that the dielectric behavior of the actual PI blocks is dominantly affected by this requirement, and the spatial confinement itself gives only a minor effect.[35]

However, it is still informative to examine this effect of the spatial confinement on the dielectric behavior of the knotted chains. The relaxation time τ_l remains the same (eq B9), and the relaxation mode distribution becomes only slightly narrower with increasing number of the chains in the knot, g. However, nonnegligible changes are observed for the dielectric intensity $\Delta\epsilon \propto \Delta C^{\parallel}(0)$; $\Delta\epsilon$ of the bundle (knotted loops/bridges) first increases moderately and then saturates with increasing $g \to \infty$. The increase indicates that the enhancement of the polarization of the knotted chains is more significant than the suppression of their motion when the number of the chains (g) included in a knot is not large, and the saturation reflects a cancellation of these effects for large g. In the absence of the spatial confinement, this cancellation takes place to give g-independent $\Delta\epsilon$ for any g value (eq B6). Thus, the effect of the knot is enhanced if the chains are spatially confined.

A qualitatively similar enhancement of the knot effect would occur when the chains are thermodynamically

required to preserve uniform segment density. In other words, the relaxation intensity may increase when the PI blocks in the triblock lamellae form knots.[35] This increase does not occur for the diblock lamellae in which the tail-type PI blocks cannot form knots. The increase of the dielectric intensity on annealing, observed only for the triblock lamella (Figure 6), may be related to the formation of knots by the PI blocks with annealing the specimen prepared by solvent casting. The chain conformation may have been quenched at some point during the solvent evaporation with the knot content being smaller than that at real equilibrium; this content seems to increase with annealing to the equilibrium value, thus inducing an increase of $\Delta\epsilon$.

At the same time, it should be noted that bridges and loops are conceptually not very different when they form knots; no significant difference is expected for contributions of the knotted loops and knotted bridges to static and dynamic properties (e.g., equilibrium swelling and dynamic moduli). In other words, the loops and bridges are *to be* distinguished only in the unknotted state, and the quenching of the chain conformation allows us to dielectrically distinguish the loop and bridge in this state.

Appendix C. Simulation Method

The CMA allows the simulation of dense polymer melts on a lattice.[49,50] The lattice is completely occupied by monomers, and the monomers of each chain are connected by $(N - 1)$ bonds of constant length. The chains satisfy the excluded volume condition. Two types of monomers, A and B, characterized by direct interaction parameters ϵ_{IJ} are considered in the case of copolymers. The energy of mixing is given only by the interactions of monomers of different type; therefore, it is assumed that $\epsilon_{AA} = \epsilon_{BB} = 0$ and $\epsilon_{AB} = 1$. The effective interaction energy per monomer E, calculated over the z nearest neighbors,

$$E(T) = \sum_{k=1}^{z} \epsilon_{IJ}(k) \tag{C1}$$

where indices I and J can both be A or B, will depend on the local structure.

To generate equilibrium states, a dense system of chains is subjected to motion at a given temperature. The moves are strictly cooperative: as in a dense system ($\rho = 1$), a segment of one chain can only move if other segments of different chains move simultaneously. Moving a chain element alters the local energy because the monomers are in close contact with new neighbors. An attempt to move a single monomer is assumed to define one Monte Carlo step, and the probability of motion is related to the interaction energy of the monomer in the attempted position, meaning that the repulsive interaction energy ϵ_{AB} creates a barrier for the formation of A−B contacts. The Metropolis[59] method is not used because the dynamics of the system is also of interest. At a given temperature, T, the Boltzmann factor $p = \exp(-E_{final}/k_B T)$ is compared with a random number r $(0 < r < 1)$. If $p > r$, the move is performed, and the motion of a new monomer is attempted. Because $\epsilon_{AB} > 0$, at low temperatures, the different types of monomeric units tend to separate from each other in order to reduce the number of A−B contacts and, consequently, to reduce the total energy.

The simulations are performed on a face centered cubic (fcc) lattice with bond length $a = \sqrt{2}$. The possible bond angles are $\alpha = 60°$, 90°, 120°, and 180° with degeneracy $d_\alpha = 4$, 2, 4, and 1, respectively. The coordination number of the lattice is $z = 12$, i.e., every monomer has 12 nearest neighbors. The lattice dimensions are $30 \times 30 \times 30$ sites except for the larger systems (BAB-90 and AB-45, Table 3), where a lattice of $60 \times 60 \times 60$ sites was used. In both cases, periodic boundary conditions have been employed in order to reduce boundary effects.

The system is initially equilibrated in the athermal limit, i.e., at $\epsilon_{IJ}/(k_B T) = 0$, where no interactions between monomers (except of the excluded volume constraints) are present, and subsequently cooled to the temperature $T/N = 1.0$, by a temperature jump, and equilibrated again. Starting from such a configuration, the system is cooled slowly by small temperature steps. At each temperature, the system is equilibrated and characterized by its energy, and a number of quantities describing its static properties are calculated. The system cooled to a low temperature is also observed during heating in the same way. Quantities characterizing the system are calculated only between cooperative rearrangement steps.

Besides the energy of interaction per monomer, which is calculated by eq C1, one can calculate the specific heat via the fluctuation dissipation theorem $C_V = (\langle E^2\rangle - \langle E\rangle^2)/(k_B T^2)$, where the brackets denote averages over the total energy of the system computed during the simulation. The thermodynamic state of the system can also be characterized by the effective interaction parameter

$$\chi_{eff} = \frac{(^1/_2)\langle E\rangle}{k_B T \phi_A \phi_B} \tag{C2}$$

where ϕ_A and ϕ_B are the volume fractions of monomers of type A and B in the system, respectively. $k_B = 1$ is assumed.

References and Notes

(1) Bates, F. S.; Fredrickson, G. H. *Annu. Rev. Phys. Chem.* **1990**, *41*, 525.
(2) *Thermoplastic Elastomers − A Comprehensive Review*; Legge, R., Holden, N. R., Schroeder, H. E., Eds.; Hanser Publishers: Münich, 1988.
(3) Hashimoto, T.; Shibayama, M.; Kawai, H. *Macromolecules* **1980**, *13*, 1237. Hadziioannou, G.; Skoulios, A. *Macromolecules* **1982**, *15*, 258; **1982**, *15*, 267.
(4) Matsushita, Y.; Nomura, M.; Watanabe, J.; Mogi, Y.; Noda, I.; Imai, M. *Macromolecules* **1995**, *28*, 6007.
(5) Helfand, E.; Wassermann, Z. R. In *Developments in Block Copolymers-1*; Goodman, I., Ed.; Applied Science: London, 1982.
(6) Matsen, M. W.; Schick, M. *Macromolecules* **1994**, *27*, 187.
(7) Jones, R. L.; Kane, L.; Spontak, R. J. *Chem. Eng. Sci.* **1996**, *51*, 1365.
(8) Anastasiadis, S. H.; Retsos, H.; Toprakcioglu, C.; Menelle, A.; Hadziioannou, G. *Macromolecules* **1998**, *31*, 6600.
(9) Koberstein, J. T.; Russell, T. P.; Walsh, D. J.; Pottick, L. *Macromolecules* **1990**, *23*, 877.
(10) Gehlsen, M. D.; Almdal, K.; Bates, F. S. *Macromolecules* **1992**, *25*, 939.
(11) Mayes, A. M.; Olvera de la Cruz, M. *J. Chem. Phys.* **1989**, *91*, 7228. Mayes, A. M.; Olvera de la Cruz, M. *J. Chem. Phys.* **1991**, *95*, 4670. Nakazawa, H.; Ohta, T. *Macromolecules* **1993**, *26*, 5503.
(12) Morton, M. In *Thermoplastic Elastomers − A Comprehensive Review*; Legge, R., Holden, N. R., Schroeder, H. E., Eds.; Hanser Publishers: Münich, 1988; Chapter 4, pp 67−90. Yamaoka, I.; Kimura, M. *Polymer* **1993**, *34*, 4399. Smith, S.;

Spontak, R.; Satkowski, M.; Ashraf, A.; Heape, A. K.; Lin, J. *Polymer* **1994**, *35*, 4527. Turner, M. *Macromolecules* **1995**, *29*, 6878.
(13) Bard, J.; Chung, C. In *Thermoplastic Elastomers − A Comprehensive Review*; Legge, R., Holden, N. R., Schroeder, H. E., Eds.; Hanser Publishers: Münich, 1988; Chapter 12, pp 303−324.
(14) Milner, S. T.; Witten, T. A. *Macromolecules* **1992**, *25*, 5495.
(15) Zhulina, E.; Halperin, A. *Macromolecules* **1992**, *25*, 5730.
(16) Matsen, M. W. *J. Chem. Phys.* **1995**, *102*, 3884.
(17) Li, B.; Ruckenstein, E. *Macromol. Theory Simul.* **1998**, *7*, 333.
(18) Leary, D. F.; Williams, M. C. *J. Polym. Sci., Polym. Lett. Ed.* **1970**, *8*, 335; **1973**, *11*, 345.
(19) Watanabe, H. *Macromolecules* **1995**, *25*, 5006.
(20) Stockmayer, W. H. *Pure Appl. Chem.* **1967**, *15*, 585. Stockmayer, W. H.; Burke, J. J. *Macromolecules* **1969**, *2*, 647. Adachi, K.; Kotaka, T. *Macromolecules* **1984**, *17*, 120.
(21) (a) Yao, M.-L.; Watanabe, H.; Adachi, K.; Kotaka, T. *Macromolecules* **1991**, *24*, 2955. (b) Yao, M.-L.; Watanabe, H.; Adachi, K.; Kotaka, T. *Macromolecules* **1992**, *25*, 1699.
(22) Alig, I.; Kremer, F.; Fytas, G.; Roovers, J. C. *Macromolecules* **1992**, *25*, 5277. Stühn, B.; Stickel, F. *Macromolecules* **1992**, *25*, 5306.
(23) Karatasos, K.; Anastasiadis, S. H.; Semenov, A. N.; Fytas, G.; Pitsikalis, M.; Hadjichristidis, N. *Macromolecules* **1994**, *27*, 3543.
(24) Karatasos, K.; Anastasiadis, S. H.; Floudas, G.; Fytas, G.; Pispas, S.; Hadjichristidis, N.; Pakula, T. *Macromolecules* **1996**, *29*, 1326.
(25) Because of the mixing within the finite interfacial width between the microdomains, junction point fluctuations can also be dielectrically active; the intensity of such process is, however, very small. Alig, I.; Floudas, G.; Avgeropoulos, A.; Hadjichristidis, N. *Macromolecules* **1997**, *30*, 5004.
(26) Watanabe, H.; Sato, T.; Osaki, K.; Yao, M.-L.; Yamagishi, A. *Macromolecules* **1997**, *30*, 5877.
(27) Cole, R. H. *J. Chem. Phys.* **1965**, *42*, 637.
(28) Provencher, S. W. *Comput. Phys. Commun.* **1982**, *27*, 213; **1982**, *27*, 229.
(29) Fytas, G.; Meier, G. In *Dynamic Light Scattering*, Brown, W., Ed.; Oxford University Press: Oxford, 1993; Chapter 9, p 407.
(30) Imanishi, Y.; Adachi, K.; Kotaka, T. *J. Chem. Phys.* **1988**, *89*, 7593. Liedermann, K.; Loidl, A. *J. Non-Cryst. Solids* **1993**, *155*, 26.
(31) Alvarez, F.; Alegria, A.; Colmenero, J. *J. Chem. Phys.* **1995**, *103*, 798. Schäfer, H.; Sternin, E.; Stannarius, R.; Arndt, M.; Kremer, F. *Phys. Rev. Lett.* **1996**, *76*, 2177.
(32) Bauer, M. E.; Stockmayer, W. H. *J. Chem. Phys.* **1965**, *43*, 4319. Adachi, K.; Kotaka, T. *Macromolecules* **1985**, *18*, 466. Boese, D.; Kremer, F. *Macromolecules* **1990**, *23*, 829.
(33) Adachi, K.; Kotaka, T. *Prog. Polym. Sci.* **1993**, *18*, 585.
(34) Pakula, T.; Karatasos, K.; Anastasiadis, S. H.; Fytas, G. *Macromolecules* **1997**, *30*, 8463.
(35) Watanabe, H.; Sato, T.; Osaki, K.; Matsumiya, Y..; Anastasiadis, S. H. *J. Soc. Rheol. Japan (Nihon Reoroji Gakkaishi)* **1999**, *27*, 173.
(36) Semenov, A. *Zh. Eksp. Teor. Fiz.* **1985**, *88*, 1242; *Sov. Phys. JETP* **1985**, *61*, 733. Semenov, A. *Macromolecules* **1993**, *26*, 6617.
(37) For reproducibility reasons, many samples were prepared following the same from-the-melt procedure. The dielectric data for the different samples are very similar (they almost superimpose at every temperature), thus verifying the fact that this sample preparation brings the system to the same stable state (at least within the time scale of the experiments).
(38) Hashimoto, T.; Tanaka, H.; Itoi, H.; Hasegawa, H. *Macromolecules* **1985**, *18*, 1864.
(39) Berg, V. D.; Groot, H. D.; Dijk, M. V.; Denley, D. *Polymer* **1994**, *35*, 5778.
(40) Sakurai, S.; Umeda, H.; Taie, K.; Nomura, S. *J. Chem. Phys.* **1997**, *105*, 8902.
(41) Albalak, R.; Thomas, E.; Capel, M. *Polymer* **1997**, *38*, 3819.
(42) Zielinski, J.; Spontak, R. *Macromolecules* **1992**, *25*, 653. Spontak, R.; Zielinski, J. *Macromolecules* **1992**, *25*, 663.
(43) Kock, M.; Sommer, J.; Blumen, A. *J. Chem. Phys.* **1997**, *106*, 1248.
(44) Kirkwood, J. J. *J. Chem. Phys.* **1939**, *7*, 911.
(45) Glarum, M.; Read, B.; Williams, G. *Inelastic and Dielectric Effects in Polymeric Solids*; Wiley: New York, 1960.
(46) Scaife, B. *Principles of Dielectrics*; Clarendon Press: Oxford, 1989.
(47) Frölich, H. *Trans. Faraday Soc.* **1948**, *44*, 238. Frölich, H. *Theory of Dielectrics*; Clarendon Press: Oxford, 1958.
(48) Fetters, L. J.; Lohse, D. J.; Richter, D.; Witten, T. A.; Zirkel, A. *Macromolecules* **1994**, *27*, 4639.
(49) Pakula, T. *Macromolecules* **1987**, *20*, 679. Pakula, T.; Geyler, S. *Macromolecules* **1987**, *20*, 2909.
(50) Kirst, K. U.; Kremer, F.; Pakula, T.; Hollingshurst, J. *Colloid Polym. Sci.* **1994**, *272*, 1420. Pakula, T.; Geyler, S.; Edling, T.; Boese, D. *Rheol. Acta* **1996**, *35*, 631.
(51) Gauger, A.; Weyersberg, A.; Pakula, T. *Makromol. Chem., Theory Simul.* **1987**, *2*, 531. Weyersberg, A.; Vilgis, T. A. *Phys. Rev. E* **1993**, *48*, 377.
(52) Smith, S.; Spontak, R.; Satkowski, M.; Ashraf, A.; Lin, J. *Phys. Rev. B* **1995**, *47*, 14555.
(53) According to eqs 5 and 1, for a monocrystalline structure, the correlations should have been calculated for the components of $\Delta\mathbf{R}$ and $\mathbf{R}$ parallel to the electric field $\mathbf{E}$, which for the experimental systems is parallel to the lamellar normal z. The orientation of the lamellae in the simulations is not known, and it is assumed that the calculation based on eqs 9−13 can capture the behavior.
(54) The respective κ calculated with performing the averaging over all of the chains are 2.0 ± 0.38, 2.4 ± 0.40, and 3.2 ± 0.42 for BAB-20, -30, and -60, respectively. These values are consistent with those in Table 5, within the errors of both calculations.
(55) Investigations of the dynamics of homopolymers with the CMA algorithm used here showed[49,50,56] that the critical molecular weight (M_c) for entanglement effects to become important is ∼40; therefore, the midblock of the BAB-60 triblock is below M_c.
(56) Pakula, T.; Matyjaszewski, K. *Makromol. Chem. Theory Simul.* **1996**, *5*, 987.
(57) Watanabe, H.; Matsuyama, S.; Mizutani, Y.; Kotaka, T. *Macromolecules* **1995**, *28*, 6454.
(58) Dimarzio, E. A. *J. Chem. Phys.* **1965**, *42*, 2101.
(59) Metropolis, N.; Rosenbluth, M. N.; Rosenbluth, A. W.; Teller, A. H.; Teller, E. *J. Chem. Phys.* **1953**, *21*, 1087.

MA991397Y